OPEN ACCESS

Exploring the growth of correlations in a quasi one-dimensional trapped Bose gas

New Journal of Physics
The open–access journal for physics

Exploring the growth of correlations in a quasi one-dimensional trapped Bose gas

M Eckart[1], R Walser and W P Schleich
Institute of Quantum Physics, Ulm University, D-89069 Ulm, Germany
E-mail: Michael.Eckart@uni-ulm.de

New Journal of Physics **10** (2008) 045024 (28pp)
Received 26 November 2007
Published 30 April 2008
Online at http://www.njp.org/
doi:10.1088/1367-2630/10/4/045024

Abstract. Phase correlations, density fluctuations and three-body loss rates are relevant for many experiments in quasi one-dimensional geometries. Extended mean-field theory is used to evaluate correlation functions up to third order for a quasi one-dimensional trapped Bose gas at zero and finite temperature. At zero temperature and in the homogeneous limit, we also study the transition from the weakly correlated Gross–Pitaevskii regime to the strongly correlated Tonks–Girardeau regime analytically. We compare our results with the exact Lieb–Liniger solution for the homogeneous case and find good agreement up to the cross-over regime.

[1] Author to whom any correspondence should be addressed.

Contents

1. Introduction

After the realization of Bose–Einstein condensation (BEC) of atomic gases a decade ago, the field has witnessed a remarkable diversification in research topics: from fundamental many-body physics questions to applications of ultra-cold gases as quantum sensors, interferometers, information processing and storage devices, as well as cooling agents for nano-oscillators. The persistent drive for miniaturization has led also to a growing number of experiments with surface traps, mounted on lithographically produced chips. In order to describe experiments that trap elongated atomic clouds, channel them through narrow waveguides, split and merge them repeatedly in interferometric sequences, one needs a robust theoretical description that can deal with time-dependent phenomena and that is able to describe spatially inhomogeneous systems at the dimensional crossover from three to one dimensions. However, it is clear that general purpose methods cannot deal with every question in ultimate precision. It is therefore necessary to gauge the systematics with known results to stake the limits of applicability. Thus, it is the purpose of this article to explore the growth of quantum correlations in quasi one-dimensional trapped Bose gases at a finite temperature with an extended mean-field (EMF) theory, which does include quantum fluctuations [1]. As expected, this agrees well in the weakly correlated regime and fails for strongly correlated systems, if compared to exact equilibrium results in the homogeneous limit.

The enhancement of quantum fluctuations in low-dimensional systems, has already stimulated many fascinating experiments in the context of ultracold gases [2]–[9], which explore

various aspects of the geometric transitions. Serendipitously, also most exactly solvable models of field theory are one-dimensional [10] and rest on the celebrated Bethe-ansatz invented in the 1930s. In the context of atomic Bose gases, today most prominent ones are the spatially homogeneous models of hard- and soft-core bosons on a string of Girardeau [11] as well as Lieb and Liniger [12, 13]. One of the many interesting questions which can be explored, is the cross-over from the weakly correlated Gross–Pitaevskii (GP) regime ($\gamma \ll 1$) to the strongly correlated Tonks–Girardeau (TG) regime [14, 15] ($\gamma \gg 1$). Thereby, one commonly uses the Lieb–Liniger (LL) parameter γ, cf (5), to measure the relative strength of repulsive self-energy to kinetic energy in the dilute Bose gas.

Today, we also have alternative tools available: firstly, there are exact few-body calculations, i.e. multi-channel time-dependent Hartree–Fock (MCTHF) or configuration interaction (CI) methods, which originate from atomic, molecular and nuclear physics. While originally designed for fermionic energy structure calculation, they are nowadays also applied to few-boson systems ($\approx$10–100 particles) in arbitrary trap geometries [16]–[19]. Secondly, there is now the possibility to prepare atomic gases in optical lattices, which are well described by the Bose–Hubbard model. Direct simulation methods, as well as density matrix renormalization group methods have been applied successfully [20]–[25]. Thirdly, there are stochastic multi-mode trajectory simulations [26] that also successfully address the same questions.

Irrespective of the choice of method, all need to predict experimentally accessible observables in terms of correlation functions, spatial averages or Fourier transforms thereof. Most relevant are obviously the lowest order moments of the bosonic field operator $\hat{a}_x$, which is the single particle density n_x at position x and the conjugate phase quadrature correlation function $g^{(1)}_{x,y}$. The fluctuations about the mean density are measured with the second-order density–density correlation function $g^{(2)}_{x,y}$

$$n_x = \langle \hat{a}^\dagger_x \hat{a}_x \rangle, \qquad g^{(1)}_{x,y} = \frac{\langle \hat{a}^\dagger_y \hat{a}_x \rangle}{\sqrt{n_x n_y}}, \qquad g^{(2)}_{x,y} = \frac{\langle \hat{a}^\dagger_x \hat{a}^\dagger_y \hat{a}_y \hat{a}_x \rangle}{n_x n_y}. \tag{1}$$

Here, $\langle \cdots \rangle = \mathrm{Tr}\{\cdots \rho\}$ denotes an average over the state of the system described by the many-body density operator ρ. Such second-order correlation functions have been measured experimentally [5, 6], [27]–[30], while the third-order density–density correlation

$$g^{(3)}_{x,y,z} = \frac{\langle \hat{a}^\dagger_x \hat{a}^\dagger_y \hat{a}^\dagger_z \hat{a}_z \hat{a}_y \hat{a}_x \rangle}{n_x n_y n_z}, \tag{2}$$

became observable only recently [4, 31] via the three-body recombination rate [32].

Theoretically, much attention has been directed toward second-order correlation functions [33]–[40], while less is known about the third-order correlation function. This situation has been rectified recently in [41, 42] where the diagonal behaviour of this correlation function was calculated in the framework of the LL theory. This is where the EMF theory is useful, because we can calculate arbitrary orders of the correlation function and will present calculations of the diagonal and off-diagonal behaviour of the third-order correlation function at zero as well as finite temperature. However, the EMF approach is restricted to values of the correlation parameter $\gamma \leqslant 1$, because any mean-field theory is known to fail in the strongly correlated regime.

This paper is organized as follows: in section 2, we briefly review the central ideas of the LL theory [12]. This celebrated solution of the 1D homogeneous Bose gas is an ideal benchmark for the EMF theory [37], [43]–[45], whose basic concepts are summarized in section 3.

In section 4, we specialize the kinetic equations to a quasi one-dimensional homogeneous situation at zero temperature for which analytical solutions can be found and compare correlation functions with the LL predictions. After successfully gauging our theoretical framework, we go beyond the homogeneous limit and numerically study inhomogeneous, harmonically trapped systems at finite temperatures in section 5.

2. Lieb–Liniger theory for bosons in 1D

LL theory based on the Bethe ansatz [10] describes a 1D homogeneous gas of N bosons on a ring of length L. It is one of the very few exactly solvable problems in many-body physics and provides a solution for every value of the correlation parameter γ. Even in inhomogeneous trapped systems this is very useful, if we can make the local density approximation (LDA). In the language of second quantization, the starting point for LL theory is the following Hamiltonian

$$\hat{H} = \int_0^L \mathrm{d}x\, \hat{a}_x^\dagger \left(-\frac{\hbar^2}{2m}\frac{\partial^2}{\partial x^2} + \frac{g}{2}\hat{a}_x^\dagger \hat{a}_x \right) \hat{a}_x, \tag{3}$$

where m denotes the mass of a boson and the creation and annihilation operators satisfy the usual bosonic commutation relation. With the help of the Hellmann–Feynman theorem [46], one can obtain the diagonal part ($x = y = 0$) of the translation invariant second-order correlation function $g^{(2)}_{x,y} = g^{(2)}_{\mathrm{LL}}$, introduced in (1), as

$$\frac{L}{2} g^{(2)}_{\mathrm{LL}} n^2 = \frac{\mathrm{d}E_0}{\mathrm{d}g} = \langle \Psi_0 | \frac{\mathrm{d}\hat{H}}{\mathrm{d}g} | \Psi_0 \rangle, \tag{4}$$

by differentiating the ground state energy E_0 with respect to the coupling constant g. Here, $|\Psi_0\rangle$ represents the ground state and $n = N/L$ denotes the linear particle density. It was shown by Lieb and Liniger [12] that the ground state energy only depends on the dimensionless correlation parameter γ. It is basically the ratio of the repulsive mean-field energy gn to the kinetic energy $\hbar^2/2md^2$ at an average distance $d = 1/n$. Another length scale of the problem is the healing length ξ, which equates the kinetic energy of a wavefunction at scale ξ to the mean-field energy

$$\gamma = \frac{mg}{\hbar^2 n}, \qquad \xi = \frac{\hbar}{\sqrt{2mng}}. \tag{5}$$

We call bosons weakly correlated for $\gamma \ll 1$ (GP regime) and strongly correlated for $\gamma \gg 1$ (TG regime).

In terms of this parameter, the ground state energy and second-order correlation function

$$E_0 = N\frac{\hbar^2 n^2}{2m} e(\gamma), \qquad g^{(2)}_{\mathrm{LL}} = e'(\gamma), \tag{6}$$

are given in terms of the solutions of the LL equations

$$e(\gamma) = \frac{\gamma^3}{\lambda^3(\gamma)} \int_{-1}^{1} \mathrm{d}x\, h(x,\gamma) x^2, \tag{7}$$

$$h(x,\gamma) = \frac{1}{2\pi} + \frac{1}{\pi}\int_{-1}^{1} \mathrm{d}y\, \frac{\lambda(\gamma) h(y,\gamma)}{\lambda^2(\gamma) + (y-x)^2}, \quad \lambda(\gamma) = \gamma \int_{-1}^{1} \mathrm{d}x\, h(x,\gamma). \tag{8}$$

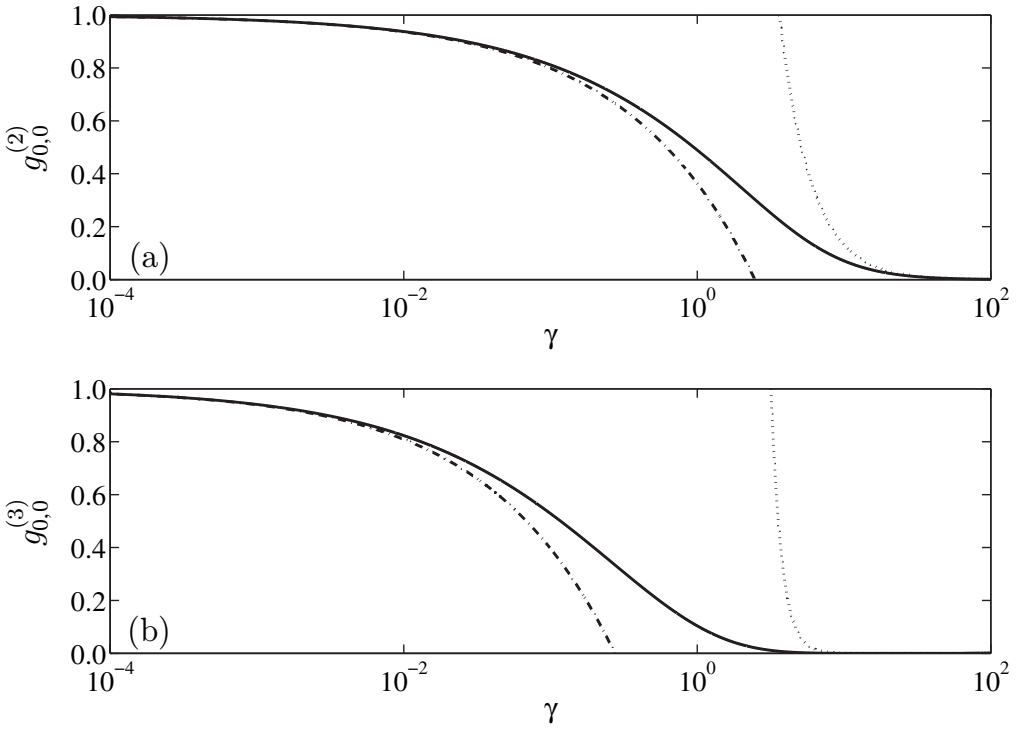

Figure 1. The LL correlation function versus the correlation parameter γ. In (a), we depict the second-order correlator $g^{(2)}_{\mathrm{LL}}$ (solid line), the GP approximation $g^{(2)}_{\mathrm{LL,GP}}$ (dashed dotted line) and the TG approximation $g^{(2)}_{\mathrm{LL,TG}}$ (dotted line), while (b) shows the third-order correlator $g^{(3)}_{\mathrm{LL}}$ (solid line) and the approximations $g^{(3)}_{\mathrm{LL,GP}}$ (dashed dotted line) and $g^{(3)}_{\mathrm{LL,TG}}$ (dotted line).

In the weakly correlated GP limit $\gamma \to 0$, as well as in the strongly correlated TG regime $\gamma \to \infty$, one obtains for the correlation function [36]

$$g^{(2)}_{\mathrm{LL,GP}} = 1 - \frac{2\sqrt{\gamma}}{\pi}, \text{ for } \gamma \ll 1, \qquad g^{(2)}_{\mathrm{LL,TG}} = \frac{4\pi^2}{3\gamma^2}, \text{ for } \gamma \gg 1. \tag{9}$$

A comparison of these approximations with the exact solution is presented in figure 1. The validity of these results has recently been tested experimentally over a wide range of the correlation parameter [6] and will be used to probe the EMF approach presented in the next section.

It is also possible to derive an exact result for the diagonal part of the third-order correlation function within the framework of the LL theory, however, the task is considerably more difficult. The exact result is derived in [42] by introducing a new function $\tilde{e}(\gamma)$ which has the form

$$\tilde{e}(\gamma) = \frac{\gamma^5}{\lambda^5(\gamma)} \int_{-1}^{1} \mathrm{d}x\, h(x,\gamma) x^4 \tag{10}$$

and with the help of this function one obtains

$$g^{(3)}_{\mathrm{LL}} = \frac{3\tilde{e}'(\gamma) - 4e(\gamma) - 6e(\gamma)e'(\gamma)}{2\gamma} + \left(1 + \frac{\gamma}{2}\right) e'(\gamma) + \frac{9e^2(\gamma) - 5\tilde{e}(\gamma)}{\gamma^2}. \tag{11}$$

A comparison of the exact result for the third-order correlation function with the approximations in the GP and the TG regime [36] is presented in figure 1

$$g^{(3)}_{\mathrm{LL,GP}} = 1 - \frac{6\sqrt{\gamma}}{\pi}, \text{ for } \gamma \ll 1, \qquad g^{(3)}_{\mathrm{LL,TG}} = \frac{16\pi^6}{15\gamma^6}, \text{ for } \gamma \gg 1. \tag{12}$$

3. Extended mean-field theory for bosons in 1D

3.1. Time-dependent Hartree–Fock–Bogoliubov equations (THFB)

The evolution of a weakly interacting dilute gas of bosons in three dimensions can be described by a Hamiltonian

$$\hat{H} = \int \mathrm{d}^6 xy\, \hat{a}^\dagger_{\mathbf{x}} \left[\mathcal{H}_{\mathbf{xy}} + \tfrac{1}{2} V_{\mathrm{bin}}(\mathbf{x}-\mathbf{y})\hat{a}^\dagger_{\mathbf{y}}\hat{a}_{\mathbf{y}}\right] \hat{a}_{\mathbf{x}}, \tag{13}$$

$$\mathcal{H}_{\mathbf{xy}} = \langle \mathbf{x}| \frac{\mathbf{p}^2}{2m} + V_{\mathrm{ext}}(\mathbf{x})|\mathbf{y}\rangle, \quad V_{\mathrm{ext}}(\mathbf{x}) = \tfrac{1}{2}m\omega^2 x^2 + \tfrac{1}{2}m\omega_\perp^2(y^2+z^2), \tag{14}$$

where $\mathcal{H}$ is the single-particle energy in an external potential V_{ext} and V_{bin} is the two-particle potential. As we are interested in the quasi one-dimensional limit, we will consider a cigar shaped trapping configuration (angular frequencies ω and $\omega_\perp$) with a large aspect ratio β. The energy and length scales will be set by the transverse oscillator

$$\beta = \omega_\perp/\omega \gg 1, \quad a_\perp = \sqrt{\hbar/m\omega_\perp}, \quad \varepsilon_\perp = \hbar\omega_\perp. \tag{15}$$

Conceptually, it is straightforward in the EMF theory to use real, finite range binary interaction potentials and obtain proper two-body T matrices including many-body corrections. However, for convenience, we will use the pseudo-potential approximation here

$$V_{\mathrm{bin}}(\mathbf{x}-\mathbf{y}) = \frac{4\pi\hbar^2 a_{\mathrm{s}}}{m}\delta_{\mathbf{x}-\mathbf{y}}, \tag{16}$$

where a_{s} denotes the s-wave scattering length. In order to compactify the notation, we will interchangeably use a subscript notation also for continuous functions.

EMF theory uses a reduced state description based on a set of master variables $\{i \in I|\gamma_i\}$. Basically, this implies the existence of a well-separated hierarchy of time, energy and length scales [1, 47] and leads to a rapid attenuation of correlation functions. Mathematically speaking, it allows for a selfconsistent expansion of the full many-body density matrix $\boldsymbol{\rho}$ in terms of a perturbation series of simple many-body density matrices $\boldsymbol{\sigma}^{(i)}$, which depend parametrically on the master variables

$$\boldsymbol{\rho} = \boldsymbol{\sigma}^{(0)}_{\{\gamma\}} + \boldsymbol{\sigma}^{(1)}_{\{\gamma\}} + \mathcal{O}(V^2_{\mathrm{bin}}). \tag{17}$$

This non-perturbative series in terms of the interaction potential V_{bin} has been introduced first by Chapman and Enskog in the context of kinetic theory of gases [48]. In addition to the simple series expansion, we impose a self-consistency constraint such that the operators $\hat{\gamma}_i$, corresponding to the c-number master variables γ_i, fulfil

$$\gamma_i = \langle\hat{\gamma}_i\rangle = \mathrm{Tr}[\hat{\gamma}_i\boldsymbol{\rho}] = \mathrm{Tr}[\hat{\gamma}_i\boldsymbol{\sigma}^{(0)}_{\{\gamma\}}]. \tag{18}$$

As far as the master variables are concerned, we choose the mean-field α_x, the normal fluctuations of the single-particle density $\tilde{f}$ and the fluctuations of the anomalous two-particle correlation function $\tilde{m}$ such that

$$\langle \hat{a}_{\mathbf{x}} \rangle = \alpha_{\mathbf{x}}, \quad f^{(c)}_{\mathbf{x},\mathbf{y}} = \alpha_{\mathbf{x}} \alpha^*_{\mathbf{y}}, \quad m^{(c)}_{\mathbf{x},\mathbf{y}} = \alpha_{\mathbf{x}} \alpha_{\mathbf{y}}, \tag{19}$$

$$\langle \hat{a}^\dagger_{\mathbf{y}} \hat{a}_{\mathbf{x}} \rangle = f^{(c)}_{\mathbf{x},\mathbf{y}} + \tilde{f}_{\mathbf{x},\mathbf{y}}, \quad \langle \hat{a}_{\mathbf{y}} \hat{a}_{\mathbf{x}} \rangle = m^{(c)}_{\mathbf{x},\mathbf{y}} + \tilde{m}_{\mathbf{x},\mathbf{y}}. \tag{20}$$

A Gaussian operator $\boldsymbol{\sigma}^{(0)}_{\{\gamma\}}$ is compatible with the requirements of (18)–(20). In turn, this implies the factorizability of multi-operator products (Wick's theorem) and also yields non-Gaussian corrections by calculating the contribution of $\boldsymbol{\sigma}^{(1)}_{\{\gamma\}}$.

By studying the coordinate transformation properties of the fluctuations [49], one finds that the averages $\tilde{f}$ and $\tilde{m}$ are components of a positive semi-definite, generalized density matrix $G \geqslant 0$. Thus, the system is described by a row vector χ, containing the mean-field α as well as its complex conjugate, and by the density matrix G

$$\chi_{\mathbf{x}} = \begin{pmatrix} \alpha_{\mathbf{x}} \\ \alpha^*_{\mathbf{x}} \end{pmatrix}, \quad G_{\mathbf{x},\mathbf{y}} = \begin{pmatrix} \tilde{f}_{\mathbf{x},\mathbf{y}} & \tilde{m}_{\mathbf{x},\mathbf{y}} \\ \tilde{m}^*_{\mathbf{x},\mathbf{y}} & \delta_{\mathbf{x},\mathbf{y}} + \tilde{f}^*_{\mathbf{x},\mathbf{y}} \end{pmatrix}. \tag{21}$$

It can be shown from a Cauchy–Schwartz inequality that at $T = 0$, the generalized density matrix G obeys an idem-potency relation

$$G\sigma_3 G + G = 0, \quad \sigma_3 = \begin{pmatrix} \mathbb{1} & 0 \\ 0 & -\mathbb{1} \end{pmatrix}. \tag{22}$$

Starting with the Heisenberg equation of motion, it is straightforward to derive the equations of motion for χ and G. In order to obtain higher order correlation functions within the present approximation scheme [43, 50], like $g^{(2)}$ or $g^{(3)}$ of (1) and (2), one has to evaluate the Gaussian $\mathrm{Tr}[\cdots \boldsymbol{\sigma}^{(0)}_{\{\gamma\}}]$ as well as the non-Gaussian contributions $\mathrm{Tr}[\cdots \boldsymbol{\sigma}^{(1)}_{\{\gamma\}}]$. However, it is clear that the Gaussian contribution will dominate for weak correlations. Thus, we have evaluated here only the Gaussian contributions. But already for $\gamma \approx 1$, deviations from that can be noticed.

3.2. Reduction to a quasi one-dimensional stationary configuration

In a very prolate trap, the transverse motion in the directions y and z is effectively frozen out and only amplitudes proportional to the ground state

$$\varphi_0(y, z, t) = \frac{\mathrm{e}^{-(y^2+z^2)/2a_\perp^2 - \mathrm{i}\omega_\perp t}}{\sqrt{\pi} a_\perp} \tag{23}$$

need to be considered. By projecting all three-dimensional functions onto the longitudinal axis $\mathbf{x} \to x$, one obtains the THFB for χ_x and $G_{x,x'}$

$$\mathrm{i}\hbar\partial_t \chi_x = \Pi_x \chi_x + \mathcal{O}(V^2_{\mathrm{bin}}), \quad \mathrm{i}\hbar\partial_t G_{x,x'} = \Sigma_x G_{x,x'} - \mathrm{h.c.} + \mathcal{O}(V^2_{\mathrm{bin}}), \tag{24}$$

with the following abbreviations for the single particle Hamiltonian and the self energies

$$\Pi_x = \begin{pmatrix} \Pi_N & \Pi_A \\ -\Pi^*_A & -\Pi^*_N \end{pmatrix}, \quad \Sigma_x = \begin{pmatrix} \Sigma_N & \Sigma_A \\ -\Sigma^*_A & -\Sigma^*_N \end{pmatrix}, \tag{25}$$

$$\Pi_N = \mathcal{H}_x + g f^{(c)}_{x,x} + 2g\tilde{f}_{x,x}, \quad \Sigma_N = \mathcal{H}_x + 2g f^{(c)}_{x,x} + 2g\tilde{f}_{x,x}, \tag{26}$$

$$\Sigma_A = g m^{(c)}_{x,x} + g\tilde{m}_{x,x}, \quad \Pi_A = g\tilde{m}_{x,x}, \quad \mathcal{H}_x = -\frac{\hbar^2}{2m}\partial_x^2 + \frac{1}{2\beta^2} m\omega_\perp^2 x^2. \tag{27}$$

In the course of the dimensional reduction, we had to introduce an effective one-dimensional coupling constant $g = 2\hbar\omega_\perp a_s$, which is in agreement with previous derivations [37, 51, 52]. In order to obtain the stationary solution for the time-independent fields χ_x and $G_{x,x'}$, we make the ansatz

$$\chi(t) = \mathrm{e}^{-(\mathrm{i}/\hbar)\mu t\sigma_3}\chi, \quad G(t) = \mathrm{e}^{-(\mathrm{i}/\hbar)\mu t\sigma_3} G\, \mathrm{e}^{(\mathrm{i}/\hbar)\mu t\sigma_3}, \tag{28}$$

which introduces the chemical potential μ and employs the Pauli matrix σ_3 of (22). This ansatz implies that the normal fluctuations $\tilde{f}_{x,x'}(t)$ become time-independent, while the anomalous fluctuations $\tilde{m}_{x,x'}(t)$ oscillate with twice the chemical potential. The properties of the resulting stationary HFB equation will be investigated in section 4 for the case of a homogeneous gas of bosons and in section 5 for a harmonic trapping potential, both at zero and for finite temperatures.

The fact that the eigenvalue in the resulting stationary equations is indeed the chemical potential [49] can be seen from a variation of the total energy functional $\mathcal{E}(\alpha, \tilde{f}, \tilde{m}) = \langle \hat{H} \rangle$ given by

$$\begin{aligned}\mathcal{E} = \int \mathrm{d}x\mathrm{d}y\, \delta(x-y) \left[\alpha_y^* \left(\mathcal{H}_x + \frac{g}{2}|\alpha_x|^2\right)\alpha_x + (\mathcal{H}_y + g\,\tilde{f}_{x,y})\,\tilde{f}_{x,y}\right] \\ + \frac{g}{2}\int \mathrm{d}x \left[\left(2|\alpha_x|^2\,\tilde{f}_{x,x} + {\alpha_x}^2 \tilde{m}^*_{x,x} + \tfrac{1}{2}|\tilde{m}_{x,x}|^2\right) + \text{h.c.}\right] + \mathcal{O}(V_{\text{bin}}^2),\end{aligned} \tag{29}$$

with the constraint that the number of particles $N = \int \mathrm{d}x\,(f^{(c)}_{x,x} + \tilde{f}_{x,x})$.

4. Analytic solution for the stationary HFB equations in the homogeneous system at zero temperature

For the calculations that are presented in the following sections, we use standard parameters for ^{87}Rb in natural units of length $a_\perp$ and energy $\varepsilon_\perp$

$$\begin{aligned} &m = 1.4432 \times 10^{-25}\,\text{kg}, \quad a_s = 5.8209 \times 10^{-9}\,\text{m}, \\ &\omega_\perp = 2\pi \times 800\,\text{Hz}, \quad \omega = 2\pi \times 3\,\text{Hz}, \\ &a_\perp = 3.8128 \times 10^{-7}\,\text{m}, \quad \tilde{g} = 2a_s/a_\perp = 3.0533 \times 10^{-2}. \end{aligned} \tag{30}$$

To reach the homogeneous case, we have to decrease the influence of the external trapping potential in (27) by weakening it to the limit $\beta \gg 1$, where we can neglect it practically. Therefore, the equilibrium state should possess the same translation symmetry as the generator of the dynamics. Consequently, we can assume that the mean field is space independent $\alpha_x = \alpha$ and the density matrix only depends on relative differences $r = x - x'$

$$\chi_x = \chi, \qquad G_{x,x'} = G_{x-x'} = \int_{-\infty}^{\infty} \frac{\mathrm{d}k}{2\pi}\, \mathrm{e}^{-\mathrm{i}kr}\mathcal{G}_k. \tag{31}$$

Translation invariant systems are best described in Fourier space, which was introduced above. We can also choose the mean field to be real-valued by a suitable phase rotation. This is a consequence of the global number conservation that is built into the dynamical

HFB equations [53]. As the mean field is real-valued $f^{(c)} = m^{(c)} = \alpha^2$, so are the fluctuations $\tilde{f}_0 = \tilde{f}_{x,x}$ and $\tilde{m}_0 = \tilde{m}_{x,x}$ and with these assumptions, the normalization constraint reads

$$n = \frac{N}{L} = f^{(c)} + \tilde{f}_0, \tag{32}$$

where n is the linear particle density on a length L. Furthermore, the THFB equations (24) simplify significantly to

$$\mu = \tilde{g}(f^{(c)} + 2\tilde{f}_0 + \tilde{m}_0), \qquad 0 = (\Sigma_k - \mu\sigma_3)\mathcal{G}_k - \text{h.c.} \tag{33}$$

From the equation for the chemical potential, it is clear that energy and length scales emerge. It will be beneficial to introduce such scales for coherence (k_c, ξ_c and ω_c), the pairing correlations ($\tilde{k}$, $\tilde{\xi}$ and $\tilde{\omega}$), and their weighted sums and differences as

$$k_c = \xi_c^{-1} = \sqrt{\omega_c}, \qquad \tilde{k} = \tilde{\xi}^{-1} = \sqrt{\tilde{\omega}}, \qquad k_\pm = {\xi_\pm}^{-1} = \sqrt{\omega_\pm}, \tag{34}$$

$$\omega_c = 4\tilde{g}f^{(c)}, \qquad \tilde{\omega} = -4\tilde{g}\tilde{m}_0, \qquad \omega_\pm = \frac{\omega_c \pm \tilde{\omega}}{2}. \tag{35}$$

In particular, in the GP regime one can assume that $\omega_c \gg \tilde{\omega}$. With these definitions, one finds that the self energy is simply a 2×2 matrix in k-space with eigenvalues ω_k

$$\Sigma_k - \mu\sigma_3 = \frac{1}{2}\begin{pmatrix} k^2 + \omega_+ & \omega_- \\ -\omega_- & -k^2 - \omega_+ \end{pmatrix}, \qquad \omega_k = \tfrac{1}{2}\sqrt{(k^2 + \omega_c)(k^2 + \tilde{\omega})}. \tag{36}$$

Now, we can finally evaluate the density matrix part of the HFB equations (33). Moreover, we also have to consider the idem-potency relation of (22). It holds for the vacuum state at zero temperature and one obtains another, now quadratic relation between normal and anomalous fluctuations in k-space

$$\tilde{m}_k = -\frac{\omega_-}{k^2 + \omega_+}\left(\tfrac{1}{2} + \tilde{f}_k\right), \qquad \tilde{f}_k = \tilde{m}_k^2 - \tilde{f}_k^2. \tag{37}$$

The system of equations can be solved point-wise in k-space and leads to two solutions, one of which has to be rejected on physical grounds. Thus, we find

$$\tilde{m}_k = -\frac{\omega_-}{4\omega_k}, \qquad \tilde{f}_k = \frac{k^2 + \omega_+}{4\omega_k} - \frac{1}{2}. \tag{38}$$

The high-momentum tail of the correlation functions is responsible for the short-scale behaviour in real space. In the limit $k \to \infty$ the leading terms are

$$\tilde{m}_k \sim -\frac{\omega_-}{2k^2}, \qquad \tilde{f}_k \sim \tilde{m}_k^2. \tag{39}$$

4.1. Diagonal contributions of normal and anomalous fluctuations

In order to obtain the diagonal part of the translation invariant correlation functions $\tilde{m}_r$ and $\tilde{f}_r$ at $r = 0$, we have to evaluate the inverse Fourier transform of (31)

$$\tilde{m}_0 = -\frac{\omega_-}{8\pi}\int_{-\infty}^{\infty}\frac{\mathrm{d}k}{\omega_k}, \qquad \tilde{f}_0 = \int_{-\infty}^{\infty}\frac{\mathrm{d}k}{2\pi}\tilde{f}_k. \tag{40}$$

Serendipitously, this can be done exactly in terms of elliptic integrals [54]

$$\tilde{m}_0 = -\frac{k_c}{4\pi}\left(1 + \frac{\tilde{m}_0}{f^{(c)}}\right)K\left(1 + \frac{\tilde{m}_0}{f^{(c)}}\right), \tag{41}$$

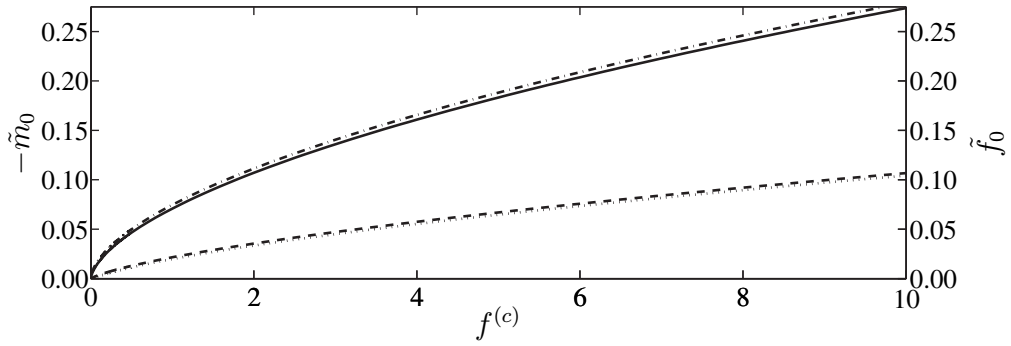

Figure 2. Diagonal part of the anomalous fluctuations $-\tilde{m}_0$ (left scale, solid line) and normal fluctuations $\tilde{f}_0$ (right scale, dashed line) versus mean field density $f^{(c)}$. The asymptotic approximations for $\tilde{m}_0$ (dashed dotted line) and $\tilde{f}_0$ (dotted line) according to (43) agree well for the considered parameter range.

$$\tilde{f}_0 = \tilde{m}_0 - \frac{k_c}{2\pi}\left[E\left(1+\frac{\tilde{m}_0}{f^{(c)}}\right) - K\left(1+\frac{\tilde{m}_0}{f^{(c)}}\right)\right], \tag{42}$$

where K and E are the complete elliptic integrals of the first and second kinds, respectively. Basic definitions are given in appendix A.1.

The scaling properties of the correlation functions are most relevant for a physical insight. Thus, we can study the GP regime of weakly correlated bosons, where $|\tilde{m}_0/f^{(c)}| \ll 1$ and use a series expansion for the elliptic integral $(1-x)K(1-x) \approx \ln(4/\sqrt{x})$. With this approximation we get

$$\tilde{m}_0 = -\frac{\sqrt{\tilde{g}f^{(c)}}}{4\pi} W\left(64\pi\sqrt{f^{(c)}/\tilde{g}}\right), \quad \tilde{f}_0 = -\frac{\sqrt{\tilde{g}f^{(c)}}}{\pi} - \tilde{m}_0. \tag{43}$$

In this explicit formula, we had to introduce the Lambert-W function, which is defined in appendix A.2 and an excellent asymptotic expansion is given in terms of logarithms [55].

The approximations for the fluctuations are compared to exact numerical calculations in figure 2 and give good agreement. We will use these approximations in the following sections to evaluate the ground state energy and correlation functions.

4.2. Off-diagonal contribution of normal and anomalous fluctuations

4.2.1. Short length scale behaviour: $r \ll \tilde{\xi}$. A rather simple, yet surprisingly efficient insight into the short-range behaviour of the off-diagonal contribution of the fluctuations can be obtained by using an iteration scheme for their Fourier transforms, which has its origin in (37). Starting with $\tilde{f}_k^{(0)} = 0$ and using the recursion relation

$$\tilde{m}_k^{(i+1)} = -\frac{\omega_-}{k^2+\omega_+}\left(\frac{1}{2}+\tilde{f}_k^{(i)}\right), \quad \tilde{f}_k^{(i+1)} = (\tilde{m}_k^{(i+1)})^2 - (\tilde{f}_k^{(i)})^2, \tag{44}$$

we get a rapid convergence towards the exact results. It is remarkable that even with the inverse Fourier transforms of low orders of this iteration scheme, we get functional behaviour for $\tilde{f}(r)$ and $\tilde{m}(r)$, which is equivalent to their exact behaviour for short ranges. However, in contrast to the exact form of the Fourier transforms of the fluctuations in (38), it is possible to perform

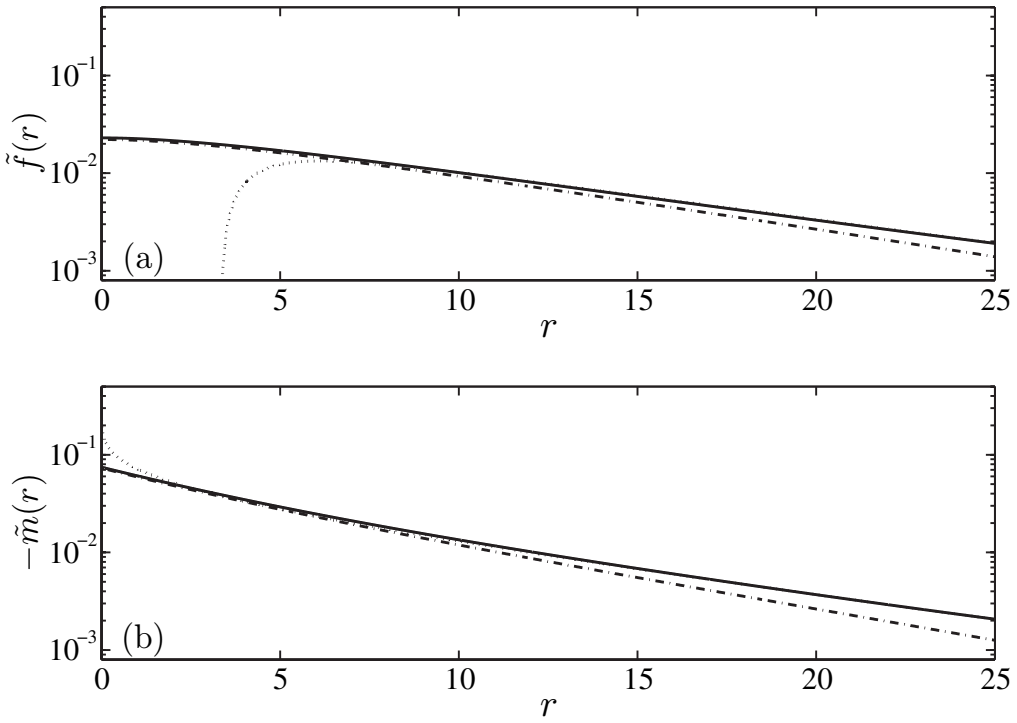

Figure 3. Off-diagonal part of the normal and anomalous fluctuations versus the distance r. In (a) we depict the normal fluctuation $\tilde{f}(r)$ (solid line), its short-range approximation $\tilde{f}^{(4)}(r)$ (dashed dotted line) and the long-range approximation (dotted line) according to (49). (b) shows the anomalous fluctuation $-\tilde{m}(r)$ (solid line), the short-range approximation $-\tilde{m}^{(4)}(r)$ thereof (dashed dotted line) and the long-range approximation (dotted line) according to (48).

the inverse Fourier transform analytically in every order of the iteration scheme. A closer look reveals that the dependence of the fluctuations on r has to be of the form

$$\tilde{m}^{(i)}(r) = \mathrm{e}^{-k_+|r|} P^{(i)}(r), \qquad \tilde{f}^{(i)}(r) = \mathrm{e}^{-k_+|r|} Q^{(i)}(r), \tag{45}$$

where $P^{(i)}(r)$ and $Q^{(i)}(r)$ are polynomials in r of order $2^i - 2$ and $2^{i+1} - 3$, respectively. Consequently, the length scale on which the correlations decay is given by

$$\xi_+ = \frac{1}{k_+} = \frac{1}{\sqrt{2\tilde{g}(f^{(c)} - \tilde{m}_0)}}. \tag{46}$$

In the GP regime, where $f^{(c)} \gg \tilde{m}_0$, we recover the healing length $\xi \approx 1/\sqrt{2\tilde{g} f^{(c)}}$, already introduced at the beginning in (5).

The short-range behaviour of the anomalous fluctuation and the normal fluctuation is depicted in figure 3. There, we compare the fourth-order result of the iteration scheme to the exact numerical evaluation of the inverse Fourier transform. We assumed $N = 100$ particles, distributed over a length of $L = 90a_\perp$. This length was chosen such that the density in the homogeneous case is similar to the density in the centre of the trapped system, which will be discussed in section 5. One obtains good agreement between the approximation and the

exact results in the regime, where $r \ll \tilde{\xi} \approx 10.5$ with $\xi \approx 3.88$. At the origin, we note that the anomalous fluctuation shows the typical cusp whereas the normal fluctuation has smooth behaviour and consequently a vanishing first derivative at $r = 0$.

4.2.2. Long length scale behaviour: $r \gg \tilde{\xi}$. In order to get an approximation for the fluctuations in this regime, we start with the Fourier transform of the anomalous fluctuation in (38) and note for further consideration that the Fourier transform of the modified Bessel function of the second kind $K_0(c|r|)$ [54] is given by $\pi/\sqrt{k^2 + c^2}$. Thus, the convolution property of the Fourier transform yields

$$\tilde{m}(r) = -\frac{\omega_-}{2\pi^2} \int_{-\infty}^{\infty} K_0(k_c|r'|) K_0(\tilde{k}|r' + r|)\, \mathrm{d}r'.$$

$K_0(r)$ diverges logarithmically at the origin and decreases exponentially for large arguments

$$K_0(r) \sim \begin{cases} -\gamma_e + \ln \frac{2}{r} + \mathcal{O}(r^2), & r \to 0, \\ \mathrm{e}^{-r} \left[\sqrt{\dfrac{\pi}{2r}} + \mathcal{O}(r^{-3/2}) \right], & r \to \infty, \end{cases} \tag{47}$$

where $\gamma_e \approx 0.5772$ denotes Euler's constant.

In the GP regime where $f^{(c)} \gg |\tilde{m}_0|$, we get from $r \gg \tilde{\xi}$ that also $r \gg \xi_c$ and therefore the first Bessel function in the integral closely resembles a δ-function. Thus, we obtain the result

$$\tilde{m}(r) = -\frac{k_c}{4\pi} \left(1 + \frac{\tilde{m}_0}{f^{(c)}} \right) K_0\left(\tilde{k}|r|\right) \approx -\frac{k_c}{4\pi} K_0\left(\tilde{k}|r|\right), \tag{48}$$

$$\tilde{f}(r) = \frac{k_c}{8\pi k_-^2} [k_c^2 K_0(\tilde{k}|r|) - \tilde{k}^2 K_2(\tilde{k}|r|)]. \tag{49}$$

An alternative derivation of this result with the help of complex integration is given in appendix B. In figure 3, the asymptotic form of the fluctuations in terms of the Bessel functions is compared to an exact numerical simulation with the parameters that were mentioned in the previous subsection. In either case the semi-logarithmic plot reveals an exponential decay for large distances $r \gg \tilde{\xi}$, in agreement with the asymptotic behaviour of the Bessel functions.

4.3. Comparison to Lieb–Liniger theory

Having all the ingredients at hand to calculate correlation functions, we are now ready for a quantitative comparison with the results of the LL theory which provides an exact solution for the behaviour of the second- and third-order correlation functions.

As outlined in section 3.1, we have to obtain the values of the correlation functions from multiple operator averages. If $\hat{o}$ is such a general operator, then

$$\langle \hat{o} \rangle = \mathrm{Tr}[\hat{o}\, (\boldsymbol{\sigma}^{(0)}_{\{\gamma\}} + \boldsymbol{\sigma}^{(1)}_{\{\gamma\}} + \mathcal{O}(\tilde{g}^2))]. \tag{50}$$

While we have already evaluated the Gaussian and non-Gaussian averages for the multinomial operator averages [43], it is clear that the Gaussian contribution will dominate for weak correlations.

Therefore, we will focus here on the Gaussian contribution and disregard the non-Gaussian contibutions in the following explicit expressions of the orders two and one, respectively

$$g^{(1)}_{x,y} = \frac{f^{(c)}_{x,y} + \tilde{f}_{x,y}}{\sqrt{n_x\, n_y}} + \mathcal{O}(\tilde{g}^2), \tag{51}$$

$$g^{(2)}_{x,y} = 1 + \frac{2\Re(\, f^{(c)}_{x,y}\, \tilde{f}_{y,x} + {m^{(c)}_{x,y}}^{*} \tilde{m}_{y,x}) + \tilde{f}_{x,y}\, \tilde{f}_{y,x} + \tilde{m}_{x,y} \tilde{m}^{*}_{y,x}}{n_x\, n_y} + \mathcal{O}(\tilde{g}), \tag{52}$$

$$\begin{aligned} g^{(3)}_{x,y} = 1 &+ \frac{2}{n_x\, n_y}\left[2\Re(\, f^{(c)}_{x,y}\, \tilde{f}_{y,x} + {m^{(c)}_{x,y}}^{*} \tilde{m}_{y,x}) + \tilde{f}_{x,y}\, \tilde{f}_{y,x} + \tilde{m}_{x,y} {\tilde{m}_{y,x}}^{*}\right] \\ &+ \frac{1}{n_x\, n_y}\left[\, f^{(c)}_{x,x}\, \tilde{f}_{y,y} + \tilde{f}_{x,x}\, \tilde{f}_{y,y} + 2\, \tilde{f}_{x,y}\, \tilde{f}_{y,x} + 2{\tilde{m}_{x,y}}^{*} \tilde{m}_{y,x}\right] \\ &+ \frac{1}{n_y^2}\left[2\Re\left(m^{(c)}_{y,y} {\tilde{m}_{y,y}}^{*}\right) + \tilde{m}_{y,y} {\tilde{m}_{y,y}}^{*} + f^{(c)}_{y,y}\, \tilde{f}_{y,y}\right] \\ &+ \frac{4}{n_x\, n_y^2}\Re\left[\, \tilde{f}_{x,y}(\tilde{m}_{y,y} {\tilde{m}_{y,x}}^{*} + m^{(c)}_{y,y} {\tilde{m}_{y,x}}^{*}) + f^{(c)}_{x,y}(\tilde{m}_{y,y} {\tilde{m}_{y,x}}^{*} + \tilde{f}_{y,y}\, \tilde{f}_{y,x}) \right. \\ &\left. + {m^{(c)}_{x,y}}(\, \tilde{f}_{y,y} {\tilde{m}_{y,x}}^{*} + {\tilde{m}_{y,y}}^{*}\, \tilde{f}_{y,x})\right] + \mathcal{O}(\tilde{g}), \end{aligned} \tag{53}$$

where $n_x = f^{(c)}_{x,x} + \tilde{f}_{x,x}$ denotes the total density. This way we can calculate the full diagonal and off-diagonal behaviour of the correlation functions. It works equally well for the trapped and homogeneous case.

In figure 4, we see a comparison of approximations and exact numerical results within the EMF theory as well as the LL theory. In either case we observe good agreement between our results and the LL theory. However, as γ increases the deviation from the exact result grows. We attribute this deviation to the non-Gaussian contributions that have been dropped.

Another relevant quantity is the ground state energy of the system. By comparing the value of the energy functional (29) with the LL ground state energy for a range of the correlation parameter γ, we obtain figure 5. In particular, we plot the relative deviation of the ground state energies. This is to be compared with deviations from a simple mean-field approach neglecting fluctuations and for the Bogoliubov method in the GP regime which includes excitations of the mean field. The latter approach results in [56]

$$e(\gamma)_{\mathrm{LL,GP}} = \gamma - \frac{4}{3\pi}\gamma^{3/2}. \tag{54}$$

In either case, we present all the results in the form of a normalized deviation from the dimensionless ground state energy $e(\gamma)$ from the LL theory given by (6).

The results show a clear improvement over simple mean-field theory and it also improves on the Bogoliubov method. Up to the cross-over at $\gamma \approx 1$, the maximum deviation of our results is less than 4% and we obtain reliable results throughout the region of interest, i.e. $\gamma \leqslant 1$. However, this appears to be the limit for a quasi one-dimensional EMF theory and different approaches have to be used in the strongly correlated regime.

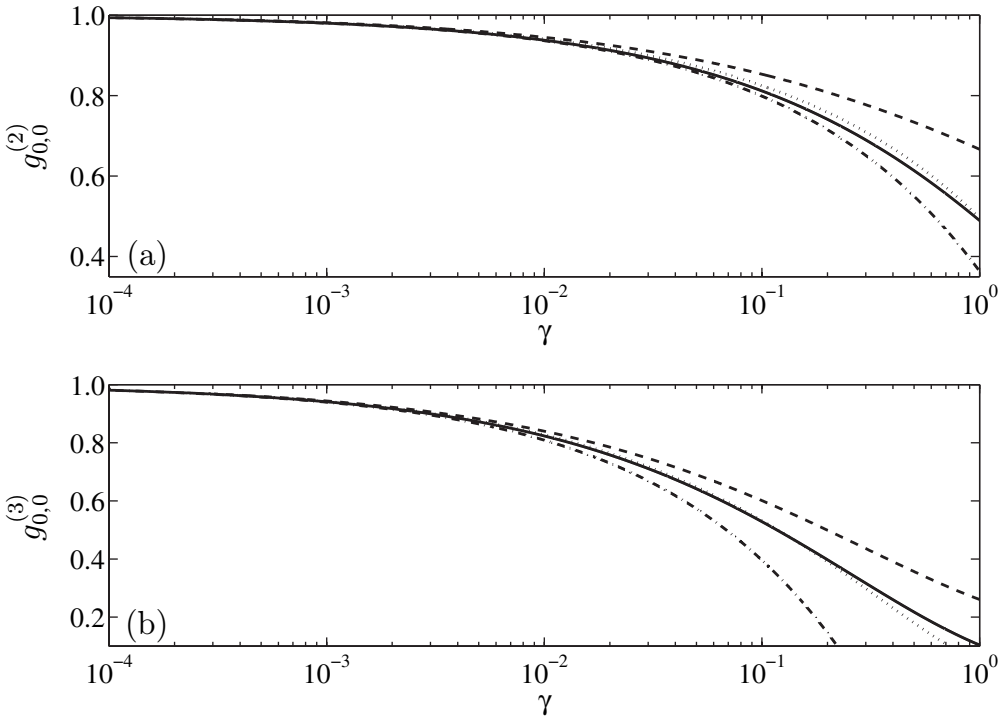

Figure 4. Second- and third-order correlation functions versus the correlation parameter γ. In (a) we compare the exact results from LL theory, $g^{(2)}_{\mathrm{LL}}$ (solid line), and the approximation in the GP regime, $g^{(2)}_{\mathrm{LL,GP}}$ (dashed dotted line) to $g^{(2)}_{x,x} \equiv g^{(2)}_{0,0}$ calculated with an EMF theory. We depict exact results (dashed line) using (41) and (42) as well as approximated results (dotted line) using (43). In (b) we depict the same comparison for the third-order correlation function.

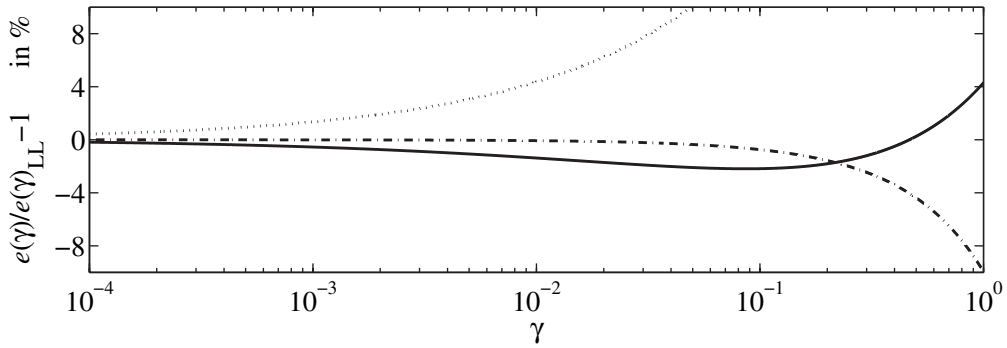

Figure 5. Relative deviations from the dimensionless ground state energy of the LL theory as a function of γ. Results from an EMF approach (solid line), the simple mean-field theory without fluctuations (dotted line) and the Bogoliubov approach (dashed dotted line) are compared.

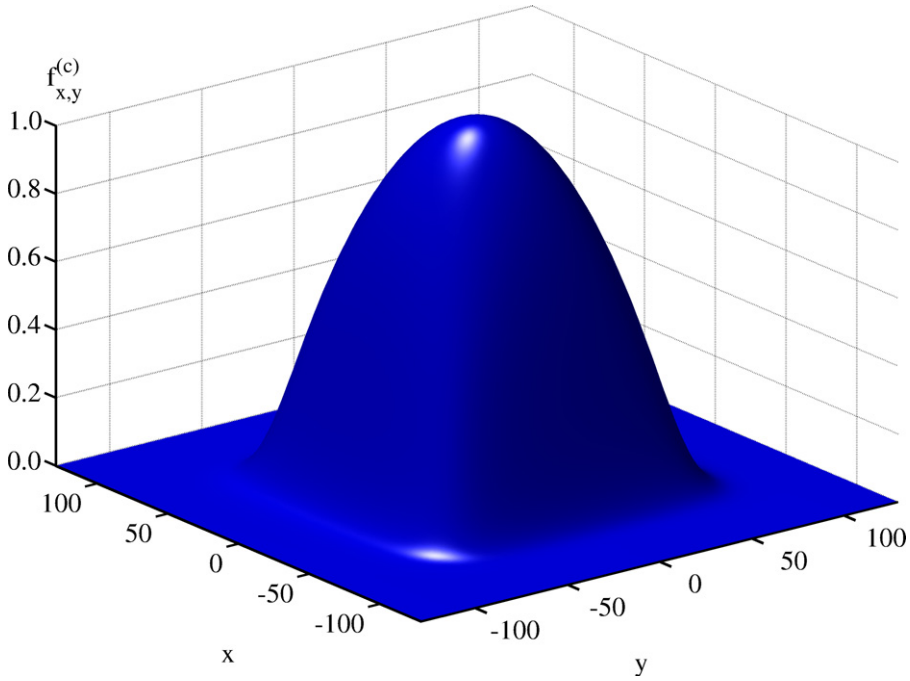

Figure 6. Coherent single-particle density matrix $f^{(c)}_{x,y}$ versus x and y. As the ground state is real valued, the coherent part of the pairing field $m^{(c)}_{x,y}$ is also represented in this figure.

5. Numerical results for trapped atoms at zero and finite temperatures

5.1. The zero temperature limit for a trapped gas

In the previous section, we have studied the homogeneous case. Here, this will be extended to harmonically trapped systems and we present correlation functions up to the third order. First of all, we depict the spatial shape of the master variables $\tilde{f}, \tilde{m}$ and of the quantities $f^{(c)}$, $m^{(c)}$, which are essential for the calculation of the correlation functions. The plots show numerical simulations for a particle number $N = 10^2$ in a trap with standard parameters for ^{87}Rb according to (30).

The coherent contribution to the single particle density matrix $f^{(c)}_{x,y}$ in figure 6 has off-diagonal long-range order and extends over the complete system. As the Hamiltonian for a one-dimensional trap is real-valued, so is the ground-state solution α_x. Hence, the coherent contribution of the pairing field $m^{(c)}_{x,y}$ is identical to $f^{(c)}_{x,y}$ and shown in figure 6.

In contrast to the coherent contributions, the normal fluctuation $\tilde{f}_{x,y}$ in figure 7 and the anomalous fluctuation $\tilde{m}_{x,y}$ in figure 8 are primarily localized along the diagonal. The coherence in the off-diagonal direction is only short range and the negativity of the pairing field is an indication of a reduced likelihood of finding two particles at the same location.

The behaviour of the first-, second- and third-order correlation functions is presented in figures 9–11. A generic feature of all three correlation functions is that they become more pronounced for smaller particle numbers. For the first-order correlation function the diagonal has to be identical to one and the deviation in the off-diagonal is fairly small as

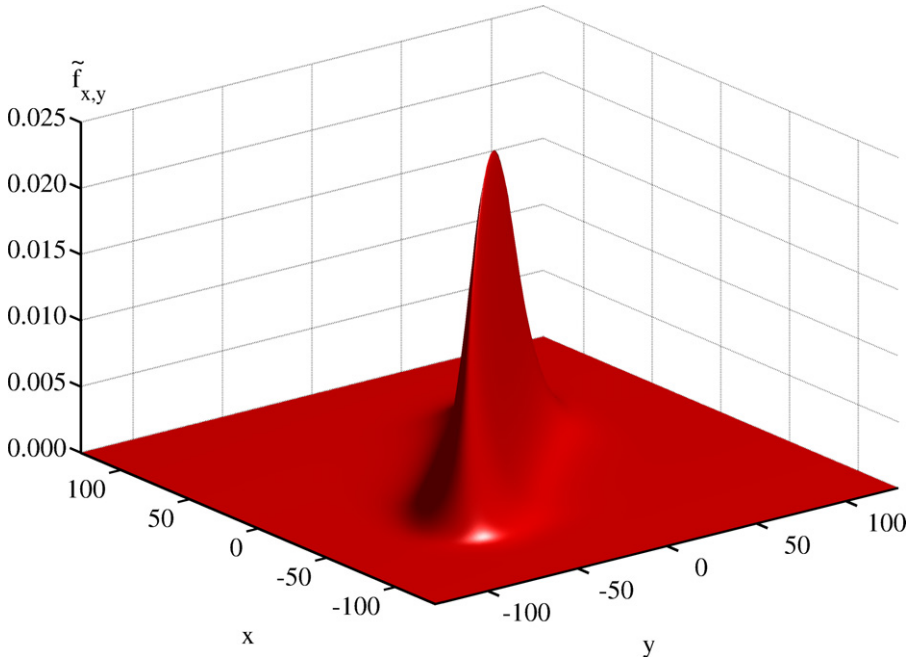

Figure 7. Normal fluctuations $\tilde{f}_{x,y}$ versus x and y.

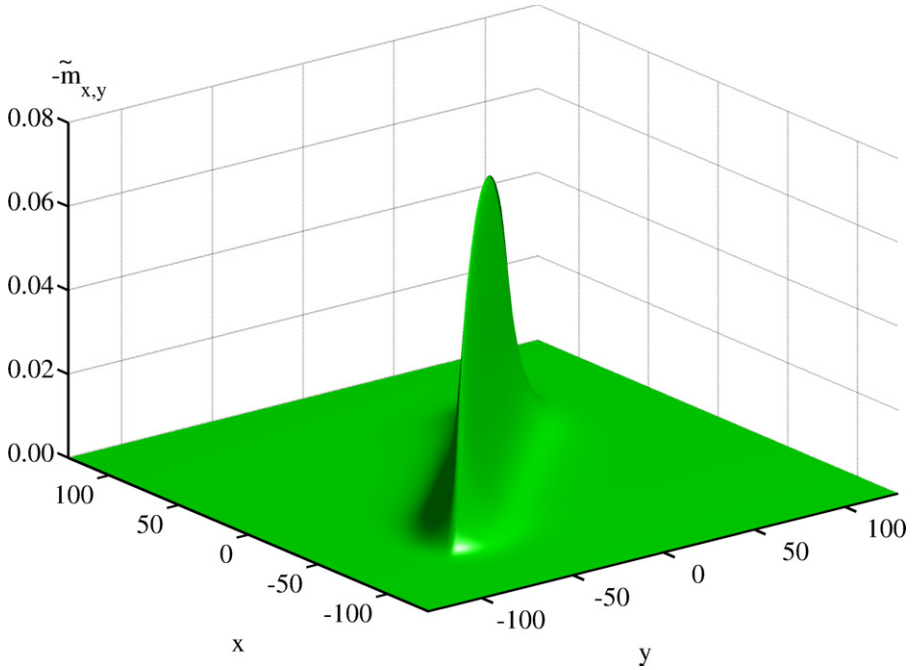

Figure 8. Anomalous fluctuations $-\tilde{m}_{x,y}$ versus x and y.

expected for a coherent system. However, the second-order, density–density correlation is a more sensitive probe as this correlation function is less than one, thus exhibiting non-classical behaviour. This anti-bunching is particularly strong for smaller particle numbers when we approach the TG regime of a fermionized Bose gas and the correlation function

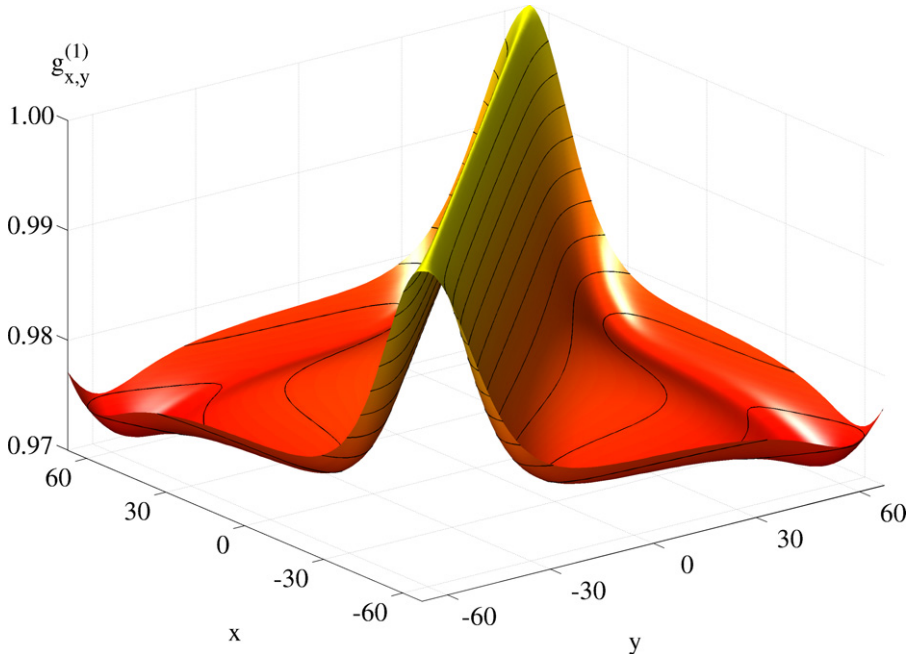

Figure 9. First-order correlation function $g^{(1)}_{x,y}$ versus x and y.

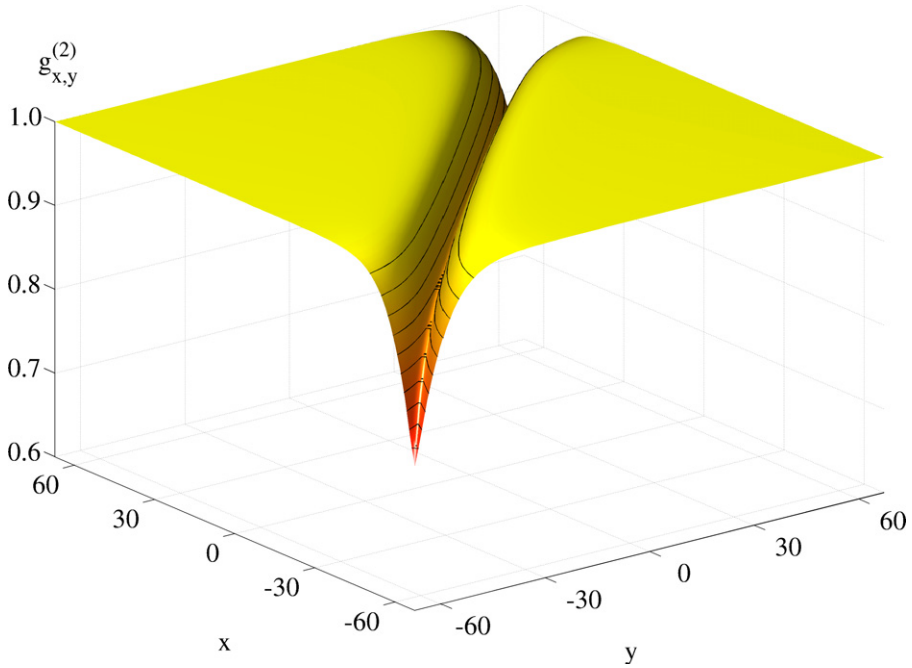

Figure 10. Second-order correlation function $g^{(2)}_{x,y}$ versus x and y.

vanishes eventually. Recently, this effect has been investigated in a number of experiments, e.g. [6, 7, 15], and the theoretical predictions have been confirmed. The same statements apply to the third-order correlation function and it can be observed that the deviation from one is even more pronounced. This also implies that the third-order correlation function [4, 31] is the most

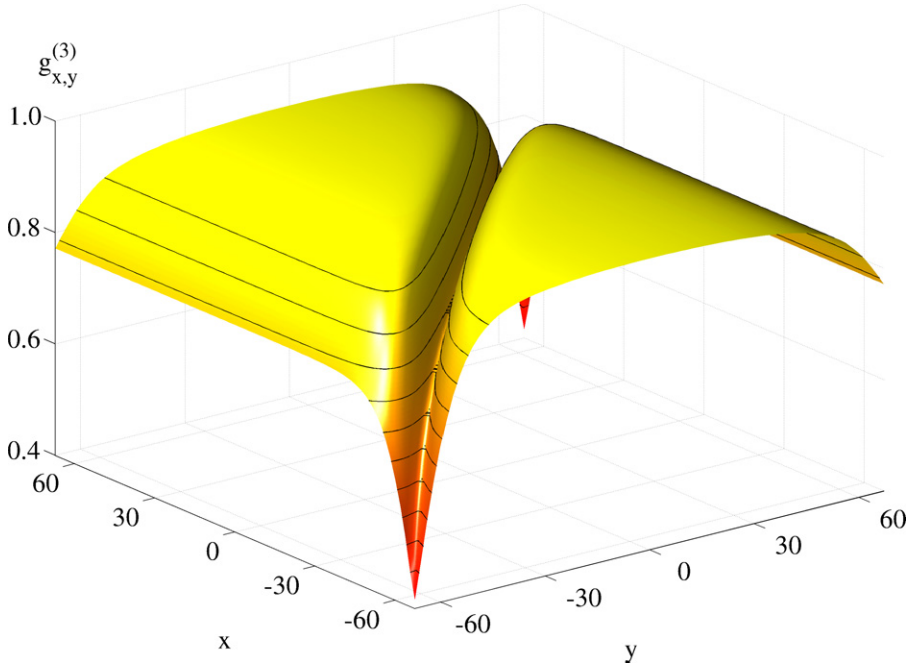

Figure 11. Third-order correlation function $g^{(3)}_{x,y}$ versus x and y.

sensitive probe for quantum aspects of the field. In addition, we notice values which are clearly below one for $|y| \gg 1$ and $x \neq y$, because in this case $g^{(3)}_{x,y} \approx g^{(2)}_{y,y}$. This can easily be seen by looking at (52) and (53) and taking into account that all the terms with off-diagonal contributions of the fluctuations in $g^{(3)}_{x,y}$ are negligible for $x \neq y$.

5.2. Behaviour in the centre of the trap

In figure 12, we compare the results of our simulations for the second- and third-order correlation functions with the LL theory. In contrast to the comparison in subsection 4.3, an external potential is now included in the calculations with the EMF theory whereas the theoretical curve is for a homogeneous gas of bosons. Our simulations are for particle numbers ranging from $N = 10^0$–10^5, and we only used the values of the correlation functions in the centre of the trap for the comparison. Compared to subsection 4.3, the results in the trapped case deviate slightly more from the exact results originating from the homogeneous LL theory but the qualitative behaviour is very similar.

5.3. Diagonal behaviour in the local density approximation

The LDA is a frequently employed approximation scheme to transfer results of homogeneous systems to spatially trapped gases. It is assumed that a smooth variation of the density profile can be incorporated by an adiabatic adjustment of a locally uniform gas. The LDA uses a local effective chemical potential [39]

$$\mu(x) = \mu_0 - V(x) = \mu_0 - \tfrac{1}{2}m\omega^2 x^2, \tag{55}$$

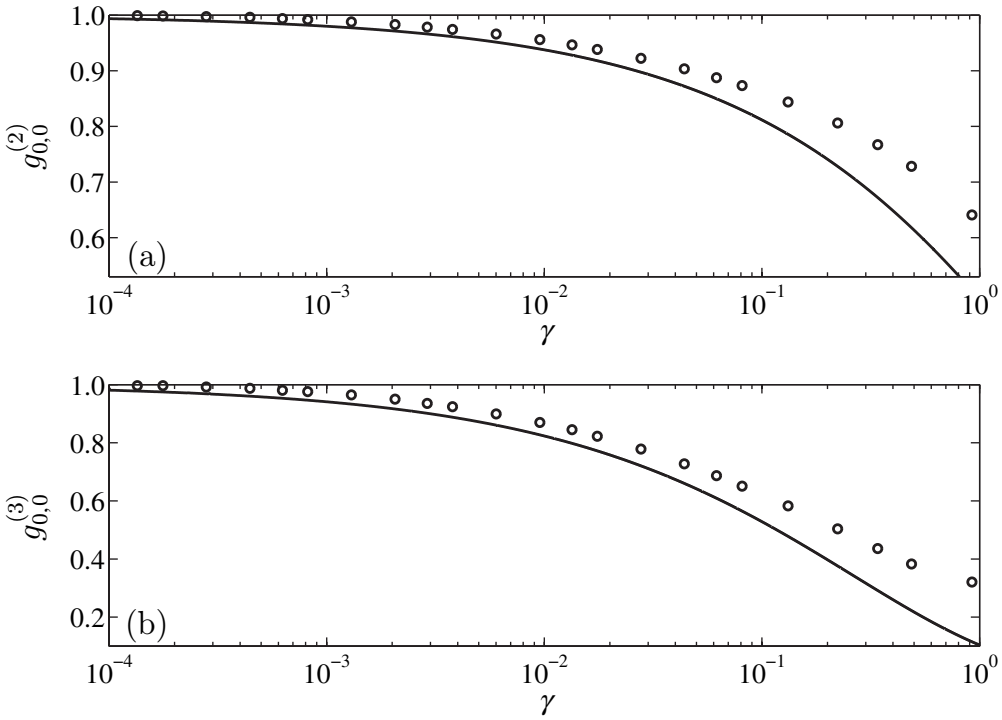

Figure 12. Correlation functions versus the correlation parameter γ. In (a) we depict $g^{(2)}_{0,0}$ and compare simulation results for the trapped case (circles) with analytic calculations obtained with LL theory (solid line). In (b) we depict $g^{(3)}_{0,0}$ and again compare simulation results for the trapped case (circles) with analytic calculations obtained with the LL theory (solid line). In both the comparisons the circles originate for particle numbers N ranging from $N = 10^5$ on the left hand side to $N = 10^0$ on the right hand side.

where μ_0 denotes the global equilibrium chemical potential. In order for the LDA to be applicable, it is thus necessary that the short-range correlation length is much smaller than the characteristic inhomogeneity length.

In this context, we want to compare the diagonal behaviour of our numerically calculated correlation functions to theoretical predictions. By definition, the first-order correlation function is identical to one along the diagonal and our data behave accordingly. For the second- and third-order correlation functions, we will compare our results with the predictions from the LL theory in the LDA. Naturally, the LDA works best in the centre of the trap. It cannot be expected to work in regions where the density drops rapidly and the inhomogeneity length is very small in these regions.

In the GP regime the chemical potential μ connects the density n to the correlation parameter γ, via

$$\mu(x) = gn(x), \qquad \gamma(x) = \frac{mg}{\hbar^2 n(x)}. \tag{56}$$

In our simulations, we tune the particle number in the trap, which decreases γ for increasing number of particles. Qualitatively, one can expect that the inhomogeneous correlation functions are higher than the homogeneous results because in the LDA the external potential

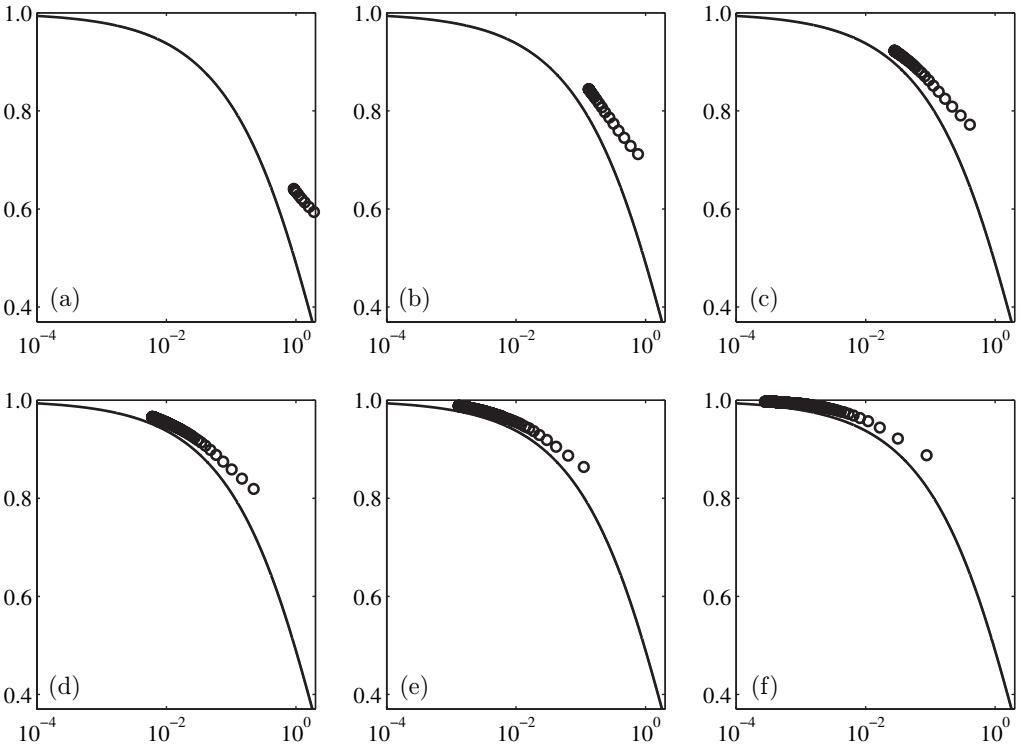

Figure 13. The diagonal second-order correlation function $g^{(2)}_{x,x}$ versus γ for various particle numbers. With an increasing value of the correlation parameter γ the circles correspond to points further outwards from the origin. We compare results for the trapped case (circles) with analytic calculations for the second-order correlation function obtained with LDA-LL theory (solid line). Plots (a)–(c) are for $N = 10^0$, 10^1 and 10^2 (from left to right) and plots (d)–(f) are for $N = 10^3$, 10^4 and 10^5 (from left to right).

leads to a smaller chemical potential and according to (56) also to a smaller density compared to the homogeneous case. Due to the monotonic decrease of the correlation functions, there is a tendency of the inhomogeneous values to be shifted to larger γ values. All the features that have just been described can be seen in figures 13 and 14, where we plotted the correlation functions for particle numbers ranging from $N = 10^0 - 10^5$ and restricted the plotted regions to the Thomas–Fermi radius.

5.4. The finite temperature result for a trapped gas

The zero-temperature results of the previous section can be extended easily to account for finite temperature effects [37, 49]. One obtains an equilibrium solution for the density matrix G of the thermal system (21) from the eigenstates of the self-energy matrix (25), according to the Bose–Einstein distribution. We present results in the present section for a particle number of $N = 100$ and a temperature $T = 10\,\hbar\omega/k_{\mathrm{B}}$.

The main thermal effect is a strong increase of the fluctuations at the edge of the trap at the cost of a reduction of the condensate density [57]. This effect is clearly seen by comparing the first-order correlation function in figure 15 to the zero temperature result in figure 9. At finite

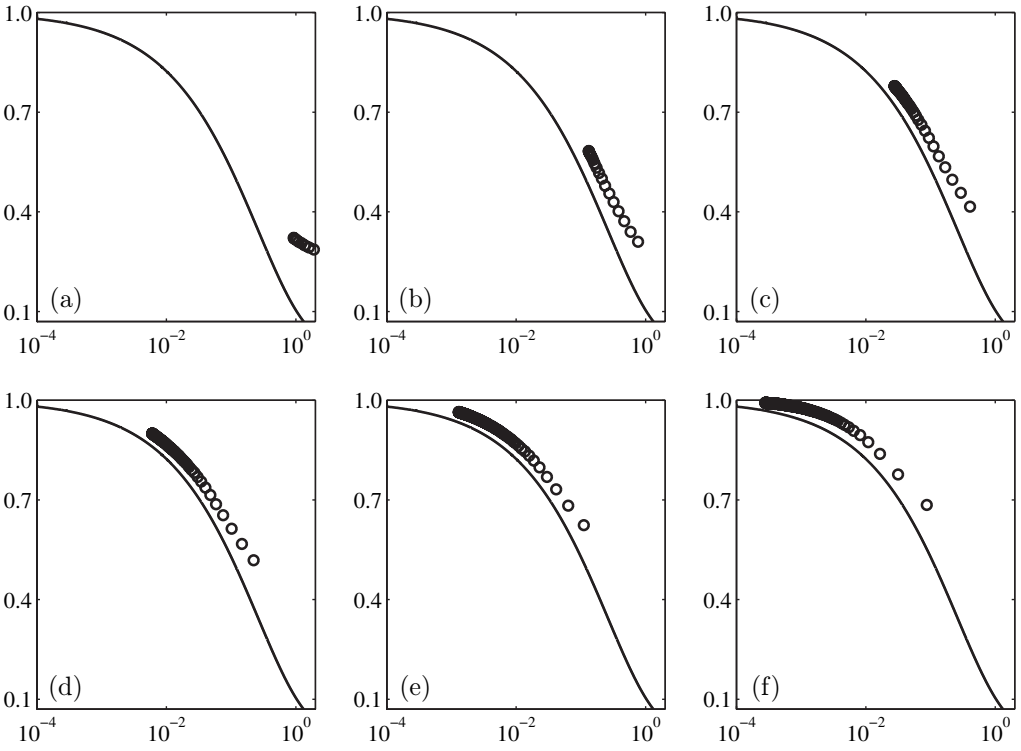

Figure 14. The diagonal third-order correlation function $g^{(3)}_{x,x}$ versus γ for various particle numbers. With an increasing value of the correlation parameter γ the circles correspond to points further outwards from the origin. We compare results for the trapped case (circles) with analytic calculations for the third-order correlation function obtained with the LDA–LL theory (solid line). Plots (a)–(c) are for $N = 10^0$, 10^1 and 10^2 (from left to right) and plots (d)–(f) are for $N = 10^3$, 10^4 and 10^5 (from left to right).

temperatures, we also obtain a reduction of first-order coherence. Consequently, this leads to a situation where the gas is almost thermalized at the edge of the trap, whereas it is coherent in the centre. The suppression of density fluctuations, also known as anti-bunching, is also less pronounced at finite temperature. This can be seen by comparing figures 16 and 17 with figures 10 and 11, which give the zero temperature results.

For a thermal gas of noninteracting bosons, one finds $g^{(2)}_{0,0} = 2!$ and $g^{(3)}_{0,0} = 3!$. It can be seen that these values are attained at the edge of the trap where fluctuations dominate. In figure 17, we also notice a value of two for $|y| \gg 1$ and $x \neq y$, because we again have $g^{(3)}_{x,y} \approx g^{(2)}_{y,y} = 2$ in this case.

In figure 18, we present the off-diagonal of the first- and second-order correlation functions $g^{(1,2)}_{x,-x}$ versus x for temperatures from $k_B T = 0 - 10\,\hbar\omega$ in increments of $2\,\hbar\omega$. It can be noticed that correlations are strongly attenuated with increasing temperature. Looking at the off-diagonal of $g^{(2)}_{x,-x}$ in figure 18, we see a reduction of the anti-bunching dip in the centre with increasing temperature; however, it is still present for high values of the temperature. It can be understood qualitatively from the stronger increase of fluctuations with the temperature at the edge of the trap. Thus, the anti-bunching dip in the centre of the trap remains visible even at finite temperatures.

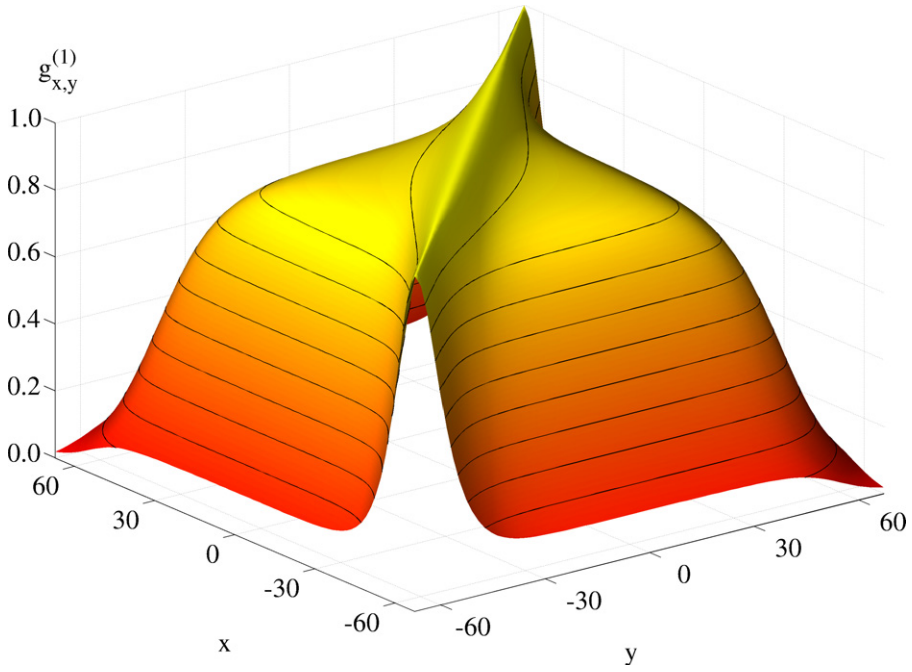

Figure 15. Finite temperature first-order correlation function $g^{(1)}_{x,y}$ versus x and y, for $N = 100$ and $T = 10\,\hbar\omega/k_{\mathrm{B}}$.

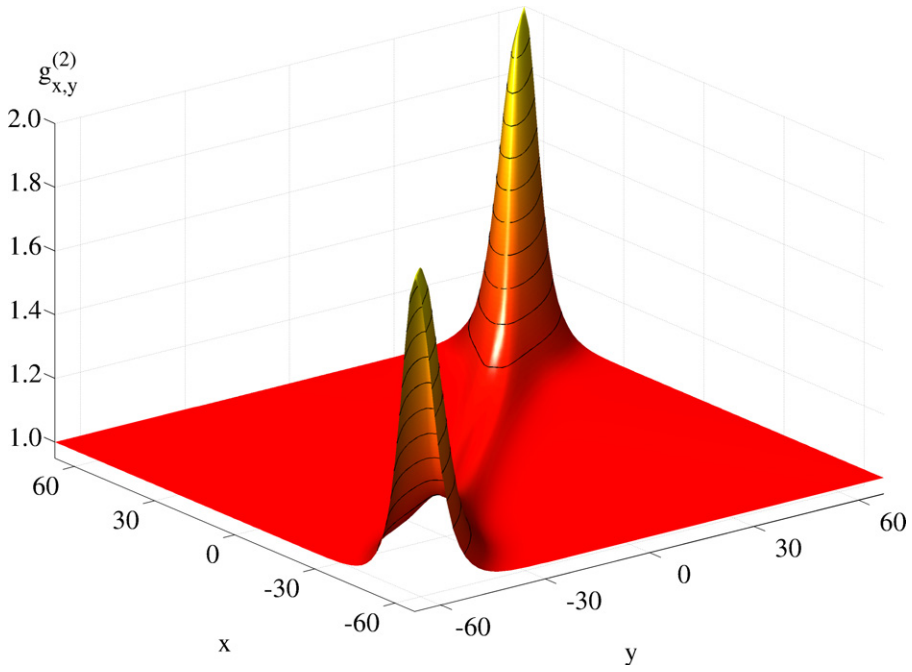

Figure 16. Finite temperature second-order correlation function $g^{(2)}_{x,y}$ versus x and y, for $N = 100$ and $T = 10\,\hbar\omega/k_{\mathrm{B}}$.

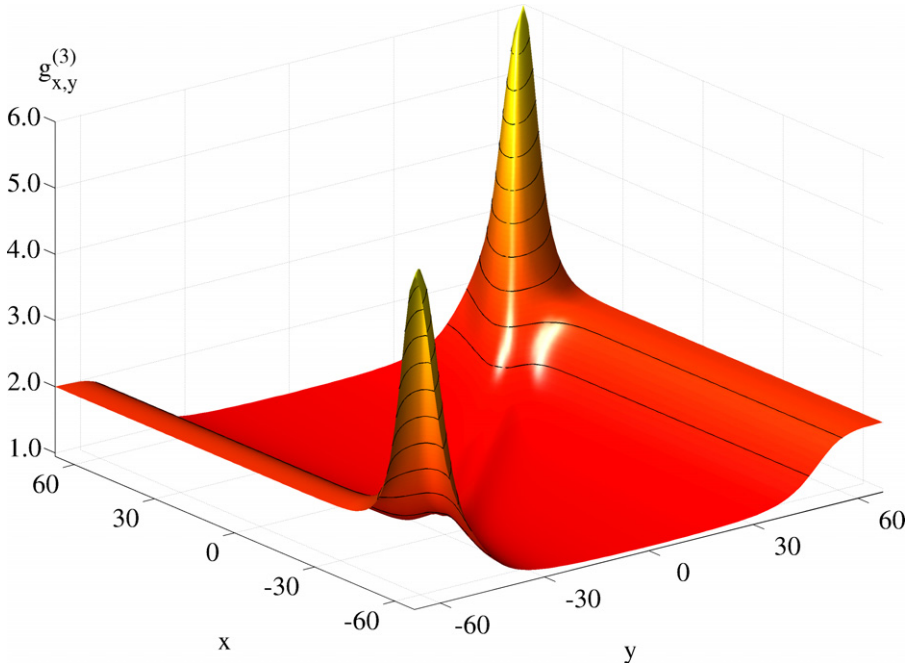

Figure 17. Finite temperature third-order correlation function $g^{(3)}_{x,y}$ versus x and y, for $N = 100$ and $T = 10\,\hbar\omega/k_{\mathrm{B}}$.

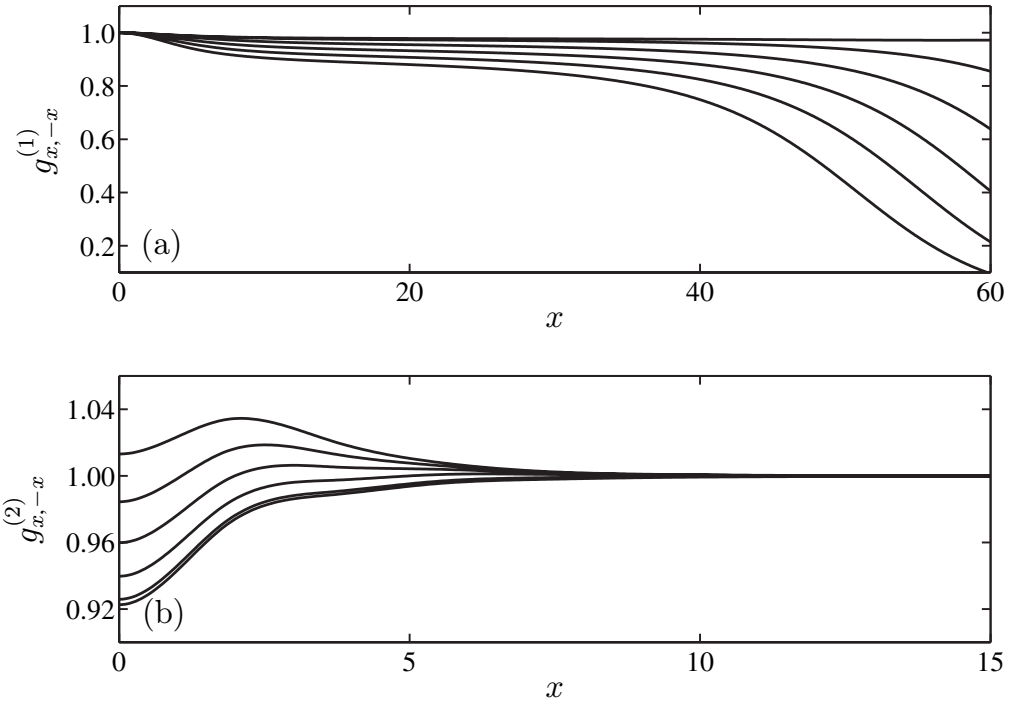

Figure 18. Off-diagonal first- $g^{(1)}_{x,-x}$ (a) and second-order correlation functions $g^{(2)}_{x,-x}$ (b) versus x. The individual curves correspond to temperatures $k_{\mathrm{B}}T = 0\,\hbar\omega$ (smallest value for $x = 0$) to $10\,\hbar\omega$ (largest value for $x = 0$) with increments of $2\,\hbar\omega$.

6. Conclusions and outlook

We have presented a detailed study of quantum correlations beyond mean-field in a trapped quasi one-dimensional Bose gas at zero and finite temperatures. In particular, we have studied the growth of quantum fluctuations from the weakly correlated regime to intermediate ranges of the correlation parameter $0 \leqslant \gamma \leqslant 1$. In the zero temperature, homogeneous limit this EMF theory agrees well with exact predictions of the LL theory.

There are many relevant applications for using this EMF theory in different geometrical configurations like a double-well potential [58, 59]. Yet another extension of our approach is the dimensional crossover out-of-equilibrium where in general the increase of available phase space volume leads to a decrease of correlations. An evaluation of such correlation functions is in progress.

Acknowledgments

We acknowledge the support by the German Research Foundation via SFB/TRR 21 which is a collaboration of the Universities of Stuttgart, Tübingen, Ulm and the Max Planck Institute for Solid State Research in Stuttgart.

Appendix A. Higher transcendental functions

A.1. Complete elliptic integrals

Following the definitions and the notation in [54], the complete elliptic integral of the first kind reads

$$K(m) = \int_0^{\pi/2} \frac{\mathrm{d}\theta}{\sqrt{1 - m\sin^2\theta}}, \tag{A.1}$$

where the parameter $0 \leqslant m \leqslant 1$. For the calculation of $\tilde{m}_0$ in section 4.1, we encounter an integral of the form

$$I_1 = \int_0^{\infty} \frac{\mathrm{d}k}{\sqrt{k^2 + \omega_\mathrm{c}}\sqrt{k^2 + \tilde{\omega}}} = \frac{K(m)}{k_\mathrm{c}}, \tag{A.2}$$

where $\omega_\mathrm{c} > \tilde{\omega}$. We can show that the evaluation of this integral leads to the complete elliptic integral of the first kind by making the substitution $k = k_\mathrm{c}\cot\theta$ and using $m = (\omega_\mathrm{c} - \tilde{\omega})/\omega_\mathrm{c}$.

Similarly, the complete elliptic integral of the second kind is defined as

$$E(m) = \int_0^{\pi/2} \sqrt{1 - m\sin^2\theta}\,\mathrm{d}\theta. \tag{A.3}$$

In order to calculate $\tilde{f}_0$ in section 4.1, we end up with the integral

$$I_2 = \int_0^{\infty} \mathrm{d}k\, \frac{\sqrt{k^2 + \omega_\mathrm{c}} - \sqrt{k^2 + \tilde{\omega}}}{\sqrt{k^2 + \tilde{\omega}}} \tag{A.4}$$

after separating the constant contribution which leads to the previously discussed integral. The same substitution as above $k = k_c \cot\theta$ simplifies the integral to the form

$$I_2 = k_c \int_0^{\pi/2} \frac{1-\sqrt{1-m\sin^2\theta}}{\sin^2\theta\sqrt{1-m\sin^2\theta}}\,\mathrm{d}\theta = -k_c\left(E(m)-K(m)\right). \tag{A.5}$$

A.2. The Lambert-W function

The Lambert-W function is implicitly defined by the solution of the transcendental equation [55]

$$z = We^W. \tag{A.6}$$

In the case of large arguments $z \gg 1$, one can use an asymptotic expansion

$$W(z) = \ell_1 - \ell_2 + \ell_2/\ell_1 + \cdots, \tag{A.7}$$

with $\ell_1 = \ln z$ and $\ell_2 = \ln z$.

Appendix B. Deformation of the integration contour in the complex plane

The results of section 4.2.2 can be derived alternatively with the help of complex integration [60]. If we take the inverse Fourier transform of the anomalous fluctuation of (38), we get

$$\tilde{m}(r) = -\frac{\omega_-}{4\pi}\int_{-\infty}^{\infty} \frac{e^{-ikr}}{\sqrt{k^2+\omega_c}\sqrt{k^2+\tilde{\omega}}}\,\mathrm{d}k\,. \tag{B.1}$$

Using the substitutions $k = \tilde{k}z$, $r' = \tilde{k}r$ and $b^2 = k_c^2/\tilde{k}^2$, this equation reduces to

$$\tilde{m}(r) = -\frac{\omega_-}{4\pi}\int_{-\infty}^{\infty} \frac{e^{-ir'z}}{\sqrt{z^2+b^2}\sqrt{z^2+1}}\,\frac{\mathrm{d}z}{\tilde{k}}\,. \tag{B.2}$$

For the evaluation of this integral we make a branch cut between $-\mathrm{i}$ and $-\mathrm{i}b$ and choose the path of integration as can be seen in figure B.1.

The contributions from C_1 and C_6 vanish if the contour is moved to infinity and the contributions from C_2 and C_5 cancel each other. The integrals along the semicircles around $-\mathrm{i}b$ and the circle around $-\mathrm{i}$ tend to zero if the radius tends to zero. Due to the branch cut the contributions from C_3 and C_4 are equal. Thus, the integral to be solved reads

$$I = \int_{-\infty}^{\infty} \frac{e^{-ir'z}\mathrm{d}z}{\sqrt{z^2+1}\sqrt{z^2+b^2}} = \int_{-ib}^{-i} \frac{2e^{-ir'z}\mathrm{d}z}{\sqrt{z^2+1}\sqrt{z^2+b^2}} \tag{B.3}$$

and by changing the variable of integration ($z = -\mathrm{i} - \mathrm{i}y$), taking into account that $b \gg 1$ in the GP regime, we get

$$I \approx 2e^{-r'}\int_0^{\infty} \frac{e^{-yr'}\mathrm{d}y}{\sqrt{2y+y^2}\sqrt{b^2-1-2y-y^2}}\,. \tag{B.4}$$

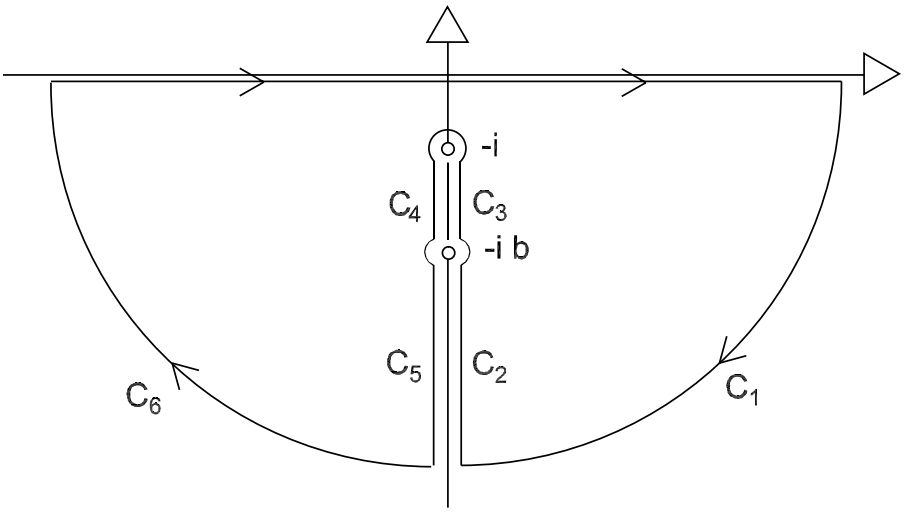

Figure B.1. Integration contour for the evaluation of (B.1).

As we are looking for an approximation for $r' = \tilde{k}r \gg 1$, we notice that only small values of y play an important role for the evaluation of the integral.

Hence, we neglect the expression $1 + 2y + y^2$ in the second term in the denominator which yields

$$I \approx 2\frac{\mathrm{e}^{-r'}}{\sqrt{b^2}} \int_0^\infty \frac{\mathrm{e}^{-yr'}}{\sqrt{2y + y^2}}\,\mathrm{d}y \;=\; \frac{2}{\sqrt{b^2}}\,K_0(r') \tag{B.5}$$

and as $\tilde{m}$ is an even function in r we get the final result

$$\tilde{m}(r) \approx -\frac{\omega_-}{2\pi k_\mathrm{c}} K_0(\tilde{k}|r|) \;\approx\; -\frac{k_\mathrm{c}}{4\pi}\,K_0(\tilde{k}|r|)\,. \tag{B.6}$$

References

[1] Akhiezer A I and Peletminskii S V 1981 *Methods of Statistical Physics* (Oxford: Pergamon)
[2] Görlitz A *et al* 2001 Realization of Bose–Einstein condensates in lower dimensions *Phys. Rev. Lett.* **87** 130402
[3] Moritz H, Stöferle T, Kohl M and Esslinger T 2003 Exciting collective oscillations in a trapped 1D gas *Phys. Rev. Lett.* **91** 250402
[4] Tolra B L, O'Hara K M, Huckans J H, Phillips W D, Rolston S L and Porto J V 2004 Observation of reduced three-body recombination in a correlated 1D degenerate Bose gas *Phys. Rev. Lett.* **92** 190401
[5] Hellweg D *et al* 2003 Measurement of the spatial correlation function of phase fluctuating Bose–Einstein condensates *Phys. Rev. Lett.* **91** 010406
[6] Kinoshita T, Wenger T and Weiss D S 2005 Local pair correlations in one-dimensional Bose gases *Phys. Rev. Lett.* **95** 190406
[7] Chuu C S, Schreck F, Meyrath T P, Hanssen J L, Price G N and Raizen M G 2005 Direct observation of sub-poissonian number statistics in a degenerate Bose gas *Phys. Rev. Lett.* **95** 260403
[8] van Amerongen A H, van Es J J P, Wicke P, Kheruntsyan K V and van Druten N J 2007 Yang–Yang thermodynamics on an atom chip *Preprint* 0709.1899
[9] Hofferberth S, Lesanovsky I, Fischer B, Schumm T and Schmiedmayer J 2007 Non-equilibrium coherence dynamics in one-dimensional Bose gases *Nature* **449** 324

[10] Mattis D C (ed) 1995 *The Many-body Problem: an Encyclopedia of Exactly Solved Models in One Dimension* (Singapore: World Scientific)
[11] Girardeau M 1960 Relationship between systems of impenetrable bosons and fermions in one dimension *J. Math. Phys.* **1** 516
[12] Lieb E and Lininger W 1963 Exact analysis of an interacting Bose gas. I. The general solution and the ground state *Phys. Rev.* **130** 1605
[13] Yang C N and Yang C P 1969 Thermodynamics of a one-dimensional system of bosons with repulsive delta-function interaction *J. Math. Phys.* **10** 1115
[14] Das K K, Girardeau M D and Wright E M 2002 Crossover from one to three dimensions for a gas of hard-core bosons *Phys. Rev. Lett.* **89** 110402
[15] Paredes B *et al* 2004 Tonks–Girardeau gas of ultracold atoms in an optical lattice *Nature* **429** 277
[16] Esry B D 1997 Hartree–Fock theory for Bose–Einstein condensate and the inclusion of correlation effects *Phys. Rev.* A **55** 1147
[17] Alon O E, Streltsov A I, Sakmann K and Cederbaum L S 2004 Continuous configuration-interaction for condensates in a ring *Europhys. Lett.* **67** 8
[18] Zöllner S, Meyer H D and Schmelcher P 2006 Correlations in ultracold trapped few-boson systems: transition from condensation to fermionization *Phys. Rev.* A **74** 063611
[19] Streltsov A I, Alon O E and Cederbaum L S 2006 General variational many-body theory with complete self-consistency for trapped bosonic systems *Phys. Rev.* A **73** 063626
[20] White S R 1992 Density matrix formulation for quantum renormalization groups *Phys. Rev. Lett.* **69** 2863
[21] Jaksch D, Bruder C, Cirac J, Gardiner C and Zoller P 1998 Cold bosonic atoms in optical lattices *Phys. Rev. Lett.* **81** 3108
[22] van Oosten D, van der Straten P and Stoof H T C 2001 Quantum phases in an optical lattice *Phys. Rev.* A **63** 053601
[23] Rigol M and Muramatsu A 2005 Fermionization in an expanding 1D gas of hard-core bosons *Phys. Rev. Lett.* **94** 240403
[24] Kollath C, Schollwöck U, von Delft J and Zwerger W 2004 Spatial correlations of trapped one-dimensional bosons in an optical lattice *Phys. Rev.* A **69** 031601
[25] Aizenman M, Lieb E H, Seiringer R, Solovej J P and Yngvason J 2004 Bose–Einstein quantum phase transition in an optical lattice model *Phys. Rev.* A **70** 023612
[26] Drummond P D and Deuar P 2003 Quantum dynamics with stochastic gauge simulations *J. Opt. B: Quantum Semiclass. Opt.* **5** S281
[27] Yasuda M and Shimizu F 1996 Observation of two-atom correlation of an ultracold neon atomic beam *Phys. Rev. Lett.* **77** 3090
[28] Bouyer P and Kasevich M 1997 Heisenberg-limited spectroscopy with degenerate Bose gases *Phys. Rev.* A **56** R1083
[29] Saubaméa B *et al* 1997 Direct measurement of the spatial correlation function of ultracold atoms *Phys. Rev. Lett.* **79** 3146
[30] Perrin A *et al* 2007 Observation of atom pairs in spontaneous four-wave mixing of two colliding Bose–Einstein condensates *Phys. Rev. Lett.* **99** 150405
[31] Burt E A, Ghrist R W, Myatt C J, Holland M J, Cornell E A and Wieman C E 1997 Coherence, correlations, and collisions: what one learns about Bose–Einstein condesates from their decay *Phys. Rev. Lett.* **79** 337
[32] Kagan Y, Svistunov B V and Shlyapnikov G V 1985 Effect of Bose condensation on inelastic processes in gases *JETP Lett.* **42** 209
[33] Petrov D S, Shlyapnikov G V and Walraven J T M 2000 Regimes of quantum degeneracy in trapped 1D gases *Phys. Rev. Lett.* **85** 3745
[34] Olshanii M and Dunjko V 2003 Short-distance correlation properties of the Lieb–Liniger system and momentum distributions of trapped one-dimensional atomic gases *Phys. Rev. Lett.* **91** 090401
[35] Gangardt D M and Shlyapnikov G V 2003 Local correlations in a strongly interacting one-dimensional Bose gas *New J. Phys.* **5** 79

[36] Gangardt D M and Shlyapnikov G V 2003 Stability and phase coherence of trapped 1D Bose gases *Phys. Rev. Lett.* **90** 010401
[37] Walser R 2004 Ground state correlations in a trapped quasi one-dimensional Bose gas *Opt. Commun.* **243** 107
[38] Bogoliubov N M, Malyshev C, Bullough R K and Timonen J 2004 Finite-temperature correlations in the one-dimensional trapped and untrapped Bose gases *Phys. Rev.* A **69** 023619
[39] Kheruntsyan K V, Gangardt D M, Drummond P D and Shlyapnikov G V 2005 Finite-temperature correlations and density profiles of an inhomogeneous interacting one-dimensional Bose gas *Phys. Rev.* A **71** 053615
[40] Astrakharchik G E and Giorgini S 2006 Correlation functions of a Lieb–Liniger Bose gas *J. Phys. B: At. Mol. Opt. Phys.* **39** S1
[41] Cheianov V V, Smith H and Zvonarev M B 2006 Exact results for three-body correlations in a degenerate one-dimensional Bose gas *Phys. Rev.* A **73** 051604
[42] Cheianov V V, Smith H and Zvonarev M B 2006 Three-body local correlation function in the Lieb–Liniger model: bosonization approach *Preprint* cond-mat/0602468
[43] Walser R, Williams J, Cooper J and Holland M 1999 Quantum kinetic theory for a condensed bosonic gas *Phys. Rev.* A **59** 3878
[44] Holland M, Park J and Walser R 2001 Formation of pairing fields in resonantly coupled atomic and molecular Bose–Einstein condensates *Phys. Rev. Lett.* **86** 1915
[45] Holland M, Kokkelmans S J J M F, Chiofalo M and Walser R 2001 Resonance superfluidity in a quantum degenerate Fermi gas *Phys. Rev. Lett.* **87** 120406
[46] Feynman R P 1939 Forces in molecules *Phys. Rev.* **56** 340
[47] Zubarev D, Morozov V and Röpke G 1997 *Statistical Mechanics of Nonequilibrium Processes Basic Concepts, Kinetic Theory* vol 1 (Berlin: Academic)
[48] Chapman S and Cowling T G 1970 *The Mathematical Theory of Non-uniform Gases* (Cambridge: Cambridge University Press)
[49] Blaizot J P and Ripka G 1986 *Quantum Theory of Finite Systems* (Cambridge, MA: MIT Press)
[50] Wachter J, Walser R, Cooper J and Holland M 2001 Equivalence of kinetic theories of Bose–Einstein condensation *Phys. Rev.* A **64** 053612
[51] Olshanii M 1998 Atomic scattering in the presence of an external confinement and a gas of impenetrable bosons *Phys. Rev. Lett.* **81** 938
[52] Menotti C and Stringari S 2002 Collective oscillations of a one-dimensional trapped Bose–Einstein gas *Phys. Rev.* A **66** 043610
[53] Griffin A 1996 Conserving and gapless approximations for an inhomogeneous Bose gas at finite temperatures *Phys. Rev.* B **53** 9341
[54] Abramowitz M and Stegun I A 1972 *Handbook of Mathematical Functions* (New York: Dover)
[55] Corless R, Gonnet G, Hare D, Jeffrey D and Knuth D 1996 On the Lambert W function *Adv. Comput. Maths.* **5** 329
[56] Wadati M 2002 Solutions of the Lieb–Liniger integral equations *J. Phys. Soc. Japan* **71** 2657
[57] Hutchinson D A W, Zaremba E and Griffin A 1997 Finite temperature excitations of a trapped Bose gas *Phys. Rev. Lett.* **78** 1842
[58] Albiez M, Gati R, Fölling J, Hunsmann S, Cristiani M and Oberthaler M K 2005 Direct observation of tunneling and nonlinear self-trapping in a single bosonic Josephson junction *Phys. Rev. Lett.* **95** 010402
[59] Gati R, Hemmerling B, Fölling J, Albiez M and Oberthaler M K 2006 Noise thermometry with two weakly coupled Bose–Einstein condensates *Phys. Rev. Lett.* **96** 130404
[60] Migdal A B 1977 *Qualitative Methods in Quantum Theory* (Reading, MA: Benjamin)